

# F-actin flow drives affinity maturation and spatial organization of LFA-1 at the immunological synapse

William A. Comrie,\* Alexander Babich,\* and Janis K. Burkhardt

Department of Pathology and Laboratory Medicine, Children's Hospital of Philadelphia and Perelman School of Medicine at the University of Pennsylvania, Philadelphia, PA 19104

Integrin-dependent interactions between T cells and antigen-presenting cells are vital for proper T cell activation, effector function, and memory. Regulation of integrin function occurs via conformational change, which modulates ligand affinity, and receptor clustering, which modulates valency. Here, we show that conformational intermediates of leukocyte functional antigen 1 (LFA-1) form a concentric array at the immunological synapse. Using an inhibitor cocktail to arrest F-actin dynamics, we show that organization of this array depends on F-actin flow and ligand mobility. Furthermore, F-actin

flow is critical for maintaining the high affinity conformation of LFA-1, for increasing valency by recruiting LFA-1 to the immunological synapse, and ultimately for promoting intracellular cell adhesion molecule 1 (ICAM-1) binding. Finally, we show that F-actin forces are opposed by immobilized ICAM-1, which triggers LFA-1 activation through a combination of induced fit and tension-based mechanisms. Our data provide direct support for a model in which the T cell actin network generates mechanical forces that regulate LFA-1 activity at the immunological synapse.

## Introduction

T cell activation and effector function require the formation of a regulated cell–cell contact with an antigen-presenting cell (APC) termed the immunological synapse (IS). IS architecture varies depending on the physiological setting and entails separation of signaling complexes into specialized membrane microdomains (Thauland and Parker, 2010). In the canonical “bullseye” IS, a distinct molecular pattern forms in which an outer ring of leukocyte functional antigen 1 (LFA-1) and talin surrounds an inner region enriched in T cell receptor (TCR) and associated signaling molecules (Monks et al., 1998; Grakoui et al., 1999). These regions have been termed the peripheral and central supramolecular activation clusters (pSMAC and cSMAC), respectively. A third distal SMAC (dSMAC) region enriched in CD45 and F-actin lies at the IS edge (Sims et al., 2007). TCR signaling occurs in microclusters that form in the IS periphery and undergo cytoskeleton-dependent translocation to the cSMAC, where signal extinction takes place (Yokosuka et al., 2005; Varma et al., 2006).

The F-actin network plays a central role in IS formation and TCR signaling (Bunnell et al., 2001; Campi et al., 2005; Varma et al., 2006; Billadeau et al., 2007; Burkhardt et al., 2008; Beemiller and Krummel, 2010; Yu et al., 2013). Actin dynamics at the IS are characterized by polymerization in the lamellipodium, centripetal flow, and filament disassembly in the central region. Centripetal flow is primarily driven by F-actin polymerization and organized by myosin IIA contraction (Babich et al., 2012; Yi et al., 2012). Simultaneous inhibition of myosin IIA contraction and F-actin polymerization arrests actin flow, with concomitant loss of  $\text{Ca}^{2+}$  signaling. Conversely, conditions that increase F-actin polymerization and centripetal flow correlate with enhanced T cell activation (Gorman et al., 2012).

Recent studies indicate that mechanical force on the TCR–peptide bound major histocompatibility antigen bond can trigger TCR signaling (Li et al., 2010; Liu et al., 2014). Further evidence for tension-based signaling comes from studies showing that T cells can respond to small numbers of monomeric ligands only when those ligands are surface bound and when their actin network is intact (Ma et al., 2008; Xie et al., 2012). Finally, T cells are known to respond differentially to stimulatory

\*W.A. Comrie and A. Babich contributed equally to this paper.

Correspondence to Janis K. Burkhardt: jburkhar@mail.med.upenn.edu

Abbreviations used in this paper: APC, antigen-presenting cell; Bleb, blebbistatin; cSMAC, central supramolecular activation cluster; dSMAC, distal SMAC; ICAM-1, intracellular cell adhesion molecule 1; IS, immunological synapse; LFA-1, leukocyte functional antigen 1; pSMAC, peripheral SMAC; SEE, staphylococcal enterotoxin E; TCR, T cell receptor; VCAM-1, vascular cell adhesion molecule 1; Y-27, Y-27632.

© 2015 Comrie et al. This article is distributed under the terms of an Attribution–Noncommercial–Share Alike–No Mirror Sites license for the first six months after the publication date (see <http://www.rupress.org/terms>). After six months it is available under a Creative Commons license (Attribution–Noncommercial–Share Alike 3.0 Unported license, as described at <http://creativecommons.org/licenses/by-nc-sa/3.0/>).

substrates of varying stiffness (Judokusumo et al., 2012; O'Connor et al., 2012). T cells in which myosin contraction has been inhibited exhibit diminished phosphorylation of CasL, a protein that undergoes stretch-dependent phosphorylation (Kumari et al., 2012). Together, these studies provide compelling evidence that the dynamic actin network plays a central role in mechanotransduction by the TCR. Nonetheless, this process remains controversial because of the lack of structure-based evidence for force-dependent TCR conformational change, and the precise role of F-actin dynamics remains unclear. Furthermore, the role of F-actin-dependent mechanical force in regulating integrins and other molecules needed for T cell activation has not been explored.

Integrins are heterodimeric transmembrane proteins that mediate cell–cell and cell–matrix interactions. The  $\alpha$ L $\beta$ 2 (CD11a/CD18) integrin LFA-1 is expressed exclusively in leukocytes and is essential for T cell trafficking and IS formation. In general, integrins are regulated at two distinct levels—valency (density at the cell–cell interface) and affinity (strength of interaction between individual integrin molecules and ligands). The overall strength of interaction (avidity) is a product of valency, affinity, and contact area (Kinashi, 2005). In resting T cells, LFA-1 is maintained in an inactive, bent conformation with very low ligand binding capacity. TCR stimulation recruits the actin binding protein talin to the  $\beta$  chain of LFA-1, relieving  $\alpha$ – $\beta$  chain interactions that maintain the bent conformation and allowing adoption of the intermediate conformation (Kim et al., 2003; Tadokoro et al., 2003; Partridge et al., 2005). This switchblade-like unfolding exposes epitopes that report on integrin activation (Fig. 1 A; Nishida et al., 2006). Signaling events that modulate LFA-1 activation are termed inside-out signaling (Kinashi, 2005; Hogg et al., 2011). Binding to ligands (intracellular cell adhesion molecule 1 [ICAM-1], 2, or 3) can also drive conformational change in a process termed “induced fit” (Takagi et al., 2002; Shimaoka et al., 2003).

Typically, integrin activation and ligand binding are associated with lateral swingout of the hybrid domain and downward movement of the  $\alpha$ 7 helix in the  $\beta$ I domain. In  $\alpha$ I domain-containing integrins such as LFA-1, this conformational change is propagated to the  $\alpha$ I domain, activating the ligand binding site (Fig. 1 A). Induction of the extended conformation results in a fourfold increase from baseline levels, and hybrid domain swingout increases affinity by an additional 100-fold. Conversely, stabilization of the closed  $\beta$ I domain decreases baseline affinity by a factor of 2. Thus, conformational change of LFA-1 regulates an 800-fold change in affinity for ICAM-1 (Schürpf and Springer, 2011). Interestingly, molecular modeling has suggested that a tensile force applied parallel to the membrane on the  $\beta$  tail can induce hybrid domain swingout and affinity modulation (Zhu et al., 2008).

Consistent with the prediction that force can enhance LFA-1 affinity, integrins engage in catch bond interactions in which force increases bond strength and longevity (Kong et al., 2009; Chen et al., 2012). Bond lifetime increases with tensile normal force until a threshold is reached after which bonds are rapidly ruptured. Importantly, this behavior depends on interactions between the  $\beta$ I and  $\alpha$ I domains, suggesting that hybrid

domain swingout is essential for catch bond interactions. Furthermore, it has been shown that integrin bond lifetimes are increased by a short, transient period of high force application. For LFA-1–ICAM-1 interactions, force cycling increased the mean bond lifetime from 1.5 to 35 s (Kong et al., 2013).

Despite the importance of integrin-dependent adhesion for T cell function, major questions remain about the mechanisms that regulate LFA-1 activation at the IS. It has been proposed that tensile force on the  $\beta$  chain can be produced via linkage to the dynamic F-actin network (Springer and Dustin, 2012), but this has not been directly tested. We have now investigated the function of the T cell actin cytoskeleton in regulating conformational change, ligand binding, and organization of LFA-1 at the IS. We show that centripetal flow of the actomyosin network is required to recruit LFA-1 to the IS, to maintain LFA-1 in the high affinity conformation, and to promote efficient binding to ICAM-1. Our data thus support a model in which mechanical force provided by F-actin centripetal flow promotes integrin-dependent T cell–APC adhesion. More generally, we show that forces generated by actin can trigger the activation of mechanosensitive molecules at the IS.

## Results

### Extended and open conformations of LFA-1 display distinct patterns of organization at the IS

T cell activation requires clustering and conformational change of LFA-1, but the distribution of LFA-1 conformational intermediates at the IS has not been characterized. To address this, we formed conjugates between human ex vivo CD4<sup>+</sup> T cells and staphylococcal enterotoxin E (SEE)–pulsed Raji B cells and labeled them with conformation-specific antibodies for LFA-1. As detailed in Materials and methods and depicted in Fig. 1 A, TS2/4 binds to  $\alpha$ L in a conformation-independent manner, Kim127 binds an epitope in the  $\beta$ 2 knee region that is exposed in the extended and open (intermediate and high affinity) conformations, and m24 binds within the  $\beta$ I domain after hybrid domain swingout and therefore detects only the high affinity, open conformation. Note that labeling with m24 must be performed before fixation because the epitope is fixation sensitive. Hereafter, labeling with these three antibodies will be, respectively, designated as  $\alpha$ L (total),  $\beta$ 2 extended, and  $\beta$ 2 open. As shown in Fig. 1 B and Video 1, total LFA-1 was distributed across the IS, except for the F-actin-rich dSMAC region. In contrast, molecules in the extended conformation were enriched in a ring corresponding roughly to the pSMAC region, whereas those in the open conformation were concentrated in a second, more central ring. Similar results were obtained in naive CD8<sup>+</sup> T cells (Fig. S1 A).

To ask if formation of this pattern is a T cell–intrinsic event, we analyzed T cells interacting with planar lipid bilayers or glass coverslips functionalized with anti-CD3 and ICAM-1. A similar concentric pattern was observed in both cases (Fig. 1, C and D) except that on coverslips T cell spreading was more extensive and activated LFA-1 molecules were localized more peripherally. Quantitative analysis (Fig. 1, C and D, right)

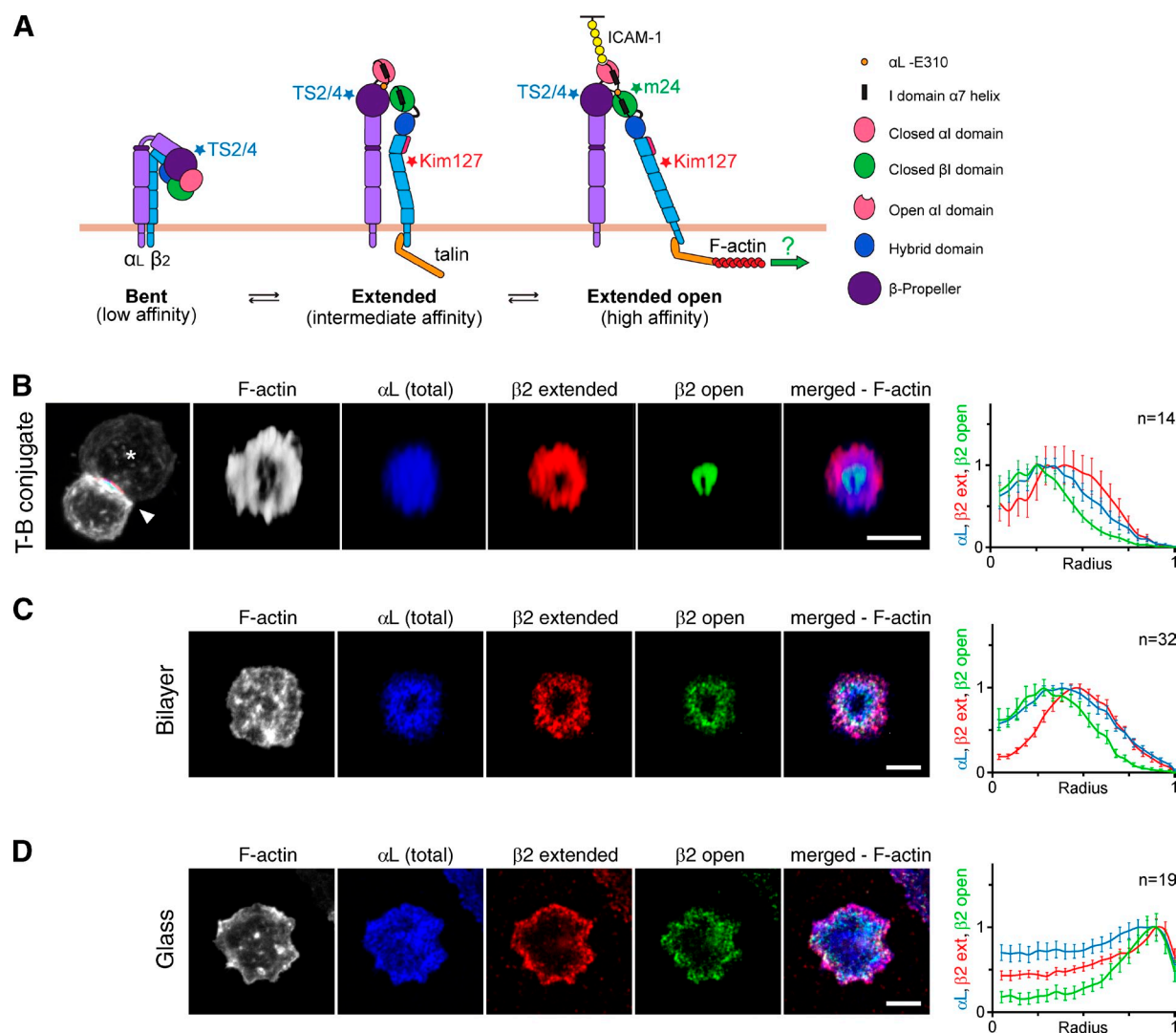


**Figure 1. LFA-1 activation intermediates are organized into a concentric array by a T cell-intrinsic mechanism.** (A) LFA-1 conformational states and antibody binding sites. Inactive LFA-1 is present in a bent conformation on the surface of T cells and exhibits low affinity for ligand. Talin binding to the  $\beta$  chain leads to unbending, yielding the extended intermediate affinity conformation. F-actin flow and ligand engagement cause the hybrid domain of the  $\beta$  chain to swing out, resulting in the high affinity extended open conformation that efficiently mediates adhesion and signaling. Putative binding sites for monoclonal antibodies are marked with asterisks. (B) Human primary CD4<sup>+</sup> T cells were conjugated to SEE-pulsed Raji B cells (asterisk) for 25 min, labeled for 5 min with m24 ( $\beta$ 2 open), and then fixed and labeled with CF405M-phalloidin to detect F-actin and monoclonal antibodies TS2/4 ( $\alpha$ L total) and Kim127 ( $\beta$ 2 extended). Z stacks of whole conjugates were collected and rendered in 3D in the IS plane (arrowhead). (right) Radial intensity profiles of synapses from multiple conjugates were analyzed as described in Materials and Methods and normalized with the maximum intensity for each antibody set equal to 1. Data represent mean  $\pm$  SEM. (C and D) Cells were allowed to spread on planar bilayers coated with anti-CD3 and 0.1  $\mu$ g/ml ICAM-1 (C) or coverglasses adsorbed with anti-CD3 and ICAM-1 (D) and analyzed as in B. Bars, 5  $\mu$ m.

confirmed the generality of these observations and highlighted the shift of the array toward the periphery in cells responding to immobilized ligand.

Previous analysis of LFA-1 activation state at the IS has relied on visualizing accumulation of laterally mobile ICAM-1 as a surrogate for engaged LFA-1 (Grakoui et al., 1999). To understand the relationship between LFA-1 conformational intermediates and ICAM-1 accumulation, we labeled T cells spreading on bilayers containing fluorescent ICAM-1. As shown in Fig. S1 (B and D), the extended conformation of LFA-1 colocalizes strongly with accumulated ICAM-1. A similar region was marked by talin, which induces the extended conformation by binding to the  $\beta$ -integrin tail (Fig. S1, F and G). m24, the antibody used to detect  $\beta$ 2 open LFA-1, has been shown to stabilize

the open LFA-1 conformation and drive accumulation of LFA-1 and ICAM-1 (Smith et al., 2005). In agreement with this, we found that incubation of cells with m24 led to increased accumulation of  $\beta$ 2 open LFA-1 over time. At early time points (1–5 min),  $\beta$ 2 open LFA-1 colocalized with only the most central region of accumulated ICAM-1 (Fig. S1, C and E), whereas by 10 min of incubation, the  $\beta$ 2 open molecules colocalized with the entire ICAM-1-rich region. The concentration of ICAM-1 in the planar bilayer influenced the overall accumulation of LFA-1 at the IS, the proportion of molecules in the extended and open conformations, and the formation of a pSMAC pattern with a central clearance (Fig. S2, B–F). Comparison of this dose-response data with the levels of ICAM-1 on the surface of mature DCs (Fig. S2 A) shows that at physiological levels of

ICAM-1 (equivalent to 0.2–0.4  $\mu\text{g/ml}$  based on labeling intensity) maximal LFA-1 accumulation and conformational change are observed. On the basis of these studies, we selected 0.3  $\mu\text{g/ml}$  of ICAM-1 and 5-min labeling with m24 as optimal conditions for further analysis.

Collectively, these results show that LFA-1 activation intermediates are organized in a concentric array at the IS, with higher affinity conformations localized more centrally. Radial organization of LFA-1 is imposed by the T cell, though the pattern is modulated by ligand density and mobility.

### ICAM-1 centralization parallels centripetal flow of the actomyosin network

We next addressed the relationship between LFA-1 conformational intermediates and the F-actin network. Human CD4<sup>+</sup> T lymphoblasts expressing Lifeact-GFP were imaged while spreading on stimulatory bilayers containing Alexa Fluor 594–ICAM-1 and Alexa Fluor 647–streptavidin bound to anti-CD3. As shown in Fig. 2 (A and B) and Video 2, ICAM-1 centralization occurred concomitantly with centripetal F-actin flow, although ICAM-1-rich features often corresponded to regions low in F-actin. This is especially evident in the kymograph shown in Video 3. Inward ICAM-1 movement stopped at the boundary with the cSMAC region marked by streptavidin. Interestingly, however, this boundary existed even in the absence of a clear streptavidin-rich region, suggesting that a mechanism other than molecular exclusion may be involved (Fig. 2 C and Video 3). Labeling of LFA-1 conformational intermediates in T lymphoblasts revealed a pattern similar to that found in ex vivo T cells; the extended conformation was enriched throughout the pSMAC region, whereas the open conformation accumulated at the pSMAC–cSMAC boundary (Fig. 2 D). Finally, we evaluated LFA-1 distribution with respect to myosin IIA because the two proteins reportedly interact (Morin et al., 2008). Myosin IIA did not colocalize with activated LFA-1, but instead localized to a region outside the rings of extended and open LFA-1 (Fig. 2 E). Thus, the distribution of LFA-1 activation intermediates cannot be explained by simple binding to F-actin or myosin IIA. Because high affinity LFA-1 preferentially binds to F-actin (Cairo et al., 2006), this conformation may be selectively delivered to the inner region of the IS by F-actin flow and deposited there upon disassembly of actin filaments. Alternatively, LFA-1 conformational change may occur as it is dragged toward the cSMAC, with maximal activation at the pSMAC–cSMAC boundary.

### Engagement of immobilized ICAM-1 retains high affinity LFA-1 at the IS periphery

We next assessed the role of ligand engagement in organizing LFA-1 activation intermediates by analyzing primary T lymphoblasts interacting with coverslips coated with anti-CD3+/–ICAM-1. As anticipated, T cells stimulated with anti-CD3+ICAM-1 spread more than cells stimulated with anti-CD3 alone (Fig. 3, A and B). In both cases, total and extended LFA-1 were enriched near the periphery of the IS, with lower intensities at the center. In contrast, ligand engagement had a dramatic effect

on the open conformation. In the presence of ICAM-1, open LFA-1 was enriched at the IS periphery, largely colocalizing with the extended conformation, but in the absence of ICAM-1 it was shifted toward the center. This pattern is similar to that observed in cells responding to planar bilayers where ICAM-1 is mobile (Compare Fig. 3 [A and B] and Fig. 1 C).

The simplest interpretation of these data is that actin-dependent delivery of open, ligand-bound LFA-1 to the center of the IS is directly opposed by immobilized ligand. However, it is also possible that binding of LFA-1 to immobilized ICAM-1 could retard actin flow, as described for  $\beta 1$  integrins (Nguyen et al., 2008). To differentiate between these possibilities, we measured F-actin flow rates in T cells responding to anti-CD3 alone or together with ICAM-1. F-actin rates were determined by kymographic analysis as detailed in Materials and methods and depicted in Video 4. T cells interacting with anti-CD3 alone showed continuous centripetal flow (Fig. 3, C–E; and Video 5, left), with rates of  $83 \pm 47$  nm/s at the IS periphery and slower rates toward the center. Addition of ICAM-1 resulted in increased F-actin at the IS center, but only modestly slowed actin flow ( $73 \pm 44$  nm/s at the periphery; Fig. 3, F–H; see Fig. S5; and Video 5, right). Thus, we favor a model in which high affinity LFA-1 binds to ICAM-1 in the periphery of the IS and is shuttled inward by actin flow. If ICAM-1 is present and immobilized, high affinity LFA-1 is physically retained in the periphery, whereas if ICAM-1 is absent or mobile, high affinity LFA-1 centralizes more extensively.

### F-actin flow regulates the valency of LFA-1 at the IS

To test the idea that forces exerted by the T cell actin cytoskeleton regulate activity of LFA-1, we used an inhibitor cocktail that arrests F-actin flow at the IS. As we reported previously (Babich et al., 2012), inhibition of myosin with Y-27632 (Y-27) or blebbistatin (Bleb) had little effect on F-actin dynamics, but addition of jasplakinolide to myosin II-inhibited cells arrested F-actin flow (Video 6). To analyze the effect of F-actin flow on redistribution of LFA-1, T-B conjugates were treated with myosin inhibitors  $\pm$  jasplakinolide, and labeled with anti-LFA-1 antibodies as diagrammed in Fig. 4 A. Enrichment was assessed based on labeling intensity at the IS (Fig. 4 D) normalized to total cell surface intensity (Fig. S3 F). Analysis was performed on cells from multiple donors; individual measurements from one donor are shown in Fig. S3 (A–E). In untreated conjugates, 60% of total LFA-1 was concentrated at the IS, where it was relatively uniformly distributed (Fig. 4, B, C, and G). Inhibition of myosin II contraction had no obvious effect on the distribution or IS enrichment of LFA-1. In contrast, cells treated with myosin II inhibitor and jasplakinolide to freeze the actin network showed significant loss (25–30%) of LFA-1 at the IS (Fig. 4, B–D and G). Similar results were obtained in T cells spreading on stimulatory bilayers, where arrest of actin flow significantly reduced total levels of IS-associated LFA-1 (Fig. 5, B, C, and F). Collectively, these results indicate that F-actin flow continuously drives LFA-1 toward the IS, thereby increasing LFA-1 valency.



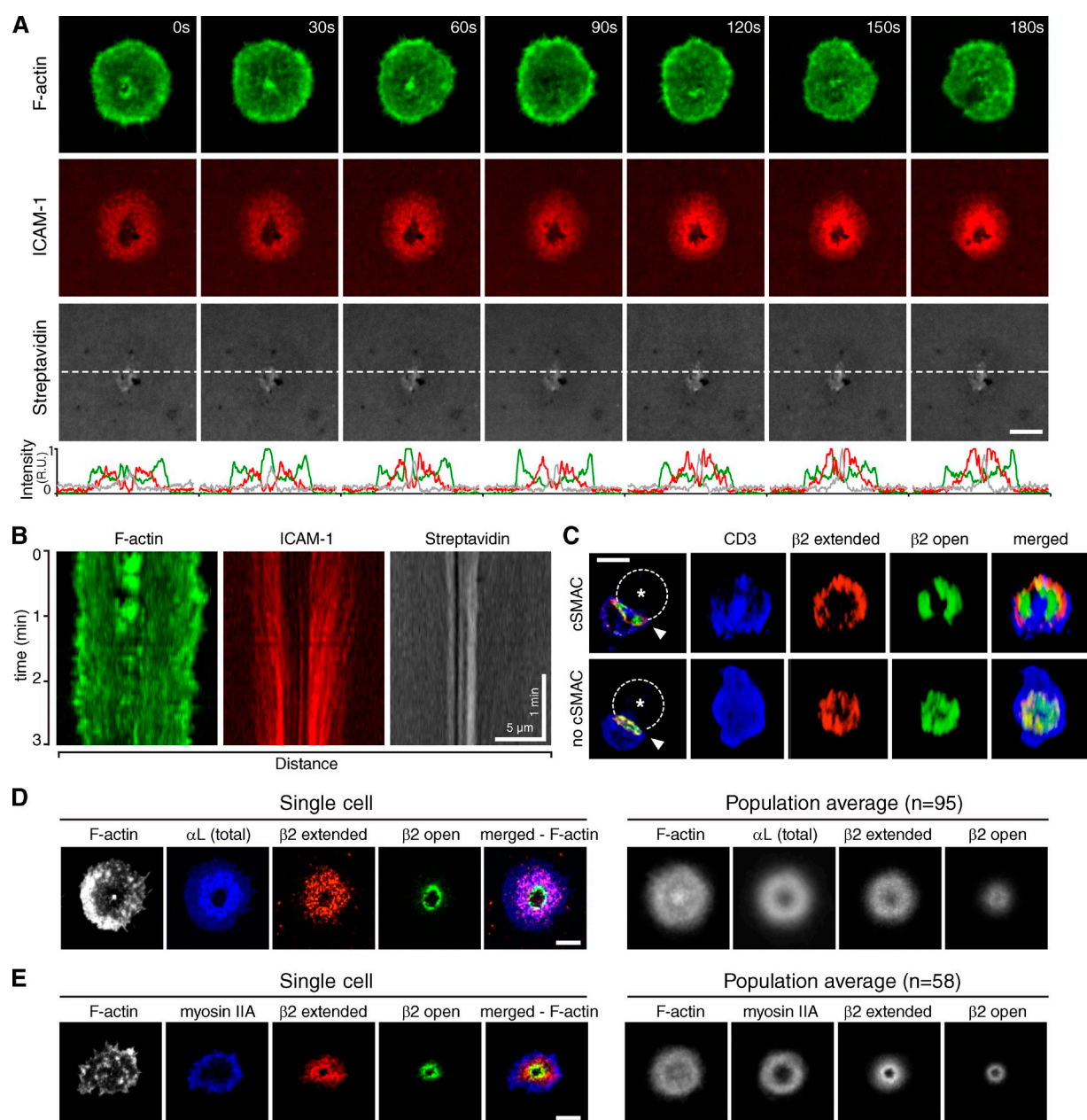


**Figure 2. Analysis of LFA-1 distribution with respect to the actomyosin network.** (A) Time-lapse series of human T lymphoblasts expressing Lifeact-GFP and spreading on planar bilayers coated with anti-CD3 linked to Alexa Fluor 647-labeled streptavidin and Alexa Fluor 594-labeled ICAM-1. Imaging was initiated after full spreading was reached. Radial profiles were generated across the indicated dotted line. Representative of 10 cells analyzed. (B) Kymographs generated from the sequence shown in A. (C) Human primary CD4<sup>+</sup> T cells were conjugated to SEE-pulsed Raji B cells (dashed outlines and asterisks) for 25 min and labeled with antibodies to the CD3 $\epsilon$  chain of TCR and to the  $\beta$ 2 chain in the extended and open conformations. Z stacks of whole conjugates were collected and rendered in 3D in the IS plane (arrowhead). Representative rendered images are shown. (D) T lymphoblasts spreading on bilayers for 30 min were labeled as in Fig. 1. Shown are single cell images and population average projections. (E) Ex vivo T cells spreading on bilayers for 30 min were labeled with conformation-specific LFA-1 and anti-myosin IIA antibodies. Bars, 5  $\mu$ m.

### Myosin II contraction and F-actin flow regulate affinity maturation of LFA-1 at the IS

To ask if the actin network regulates LFA-1 conformational change, inhibitor-dependent changes in labeling of the extended and open conformations at the IS were quantified (Fig. 4, E and F). To control for changes in valency and focus analysis on conformational change, data were normalized to labeling for total LFA-1 in the same region (Fig. 4, H and I). Note that this

arbitrary value does not indicate the actual percentage of molecules in a particular conformation, but serves as a useful measure of relative LFA-1 activation under different experimental conditions. As shown in Fig. 4 (B, C, and E), myosin II inhibition with Y-27 significantly diminished the overall amount of extended LFA-1 at the IS. Similar results were obtained with Bleb, though this did not reach statistical significance as a result of donor variability. Arrest of the actin network by addition of jasplakinolide to cells pretreated with either myosin inhibitor

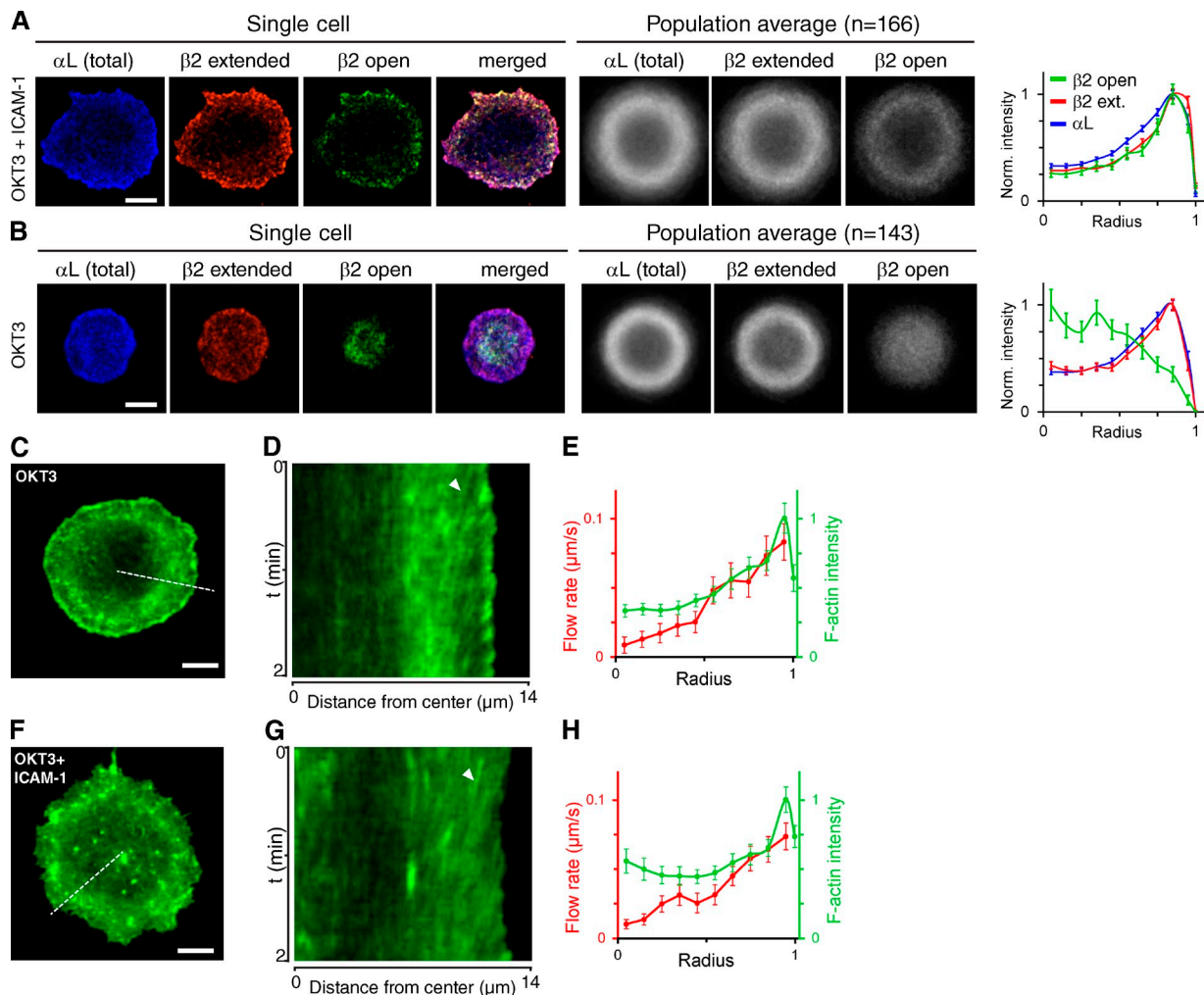


**Figure 3. ICAM-1 engagement retains the pool of activated LFA-1 in the IS periphery.** (A and B) T lymphoblasts were allowed to interact with coverslips coated with anti-CD3 and ICAM-1 (A) or anti-CD3 alone (B) for 30 min and analyzed as in Fig. 1. (C and D) T lymphoblasts expressing Lifeact-GFP were imaged live while spreading on coverslips coated with anti-CD3 alone. (C) Single time point of a responding cell and (D) corresponding kymograph of F-actin dynamics generated along the dashed line in C. Arrowhead indicates a mobile fiducial mark in the F-actin network. (E) Kymographic analysis of F-actin flow rates along IS radii (663 measurements from 13 cells) superimposed on the normalized radial distribution of F-actin intensity in the same cells. (F and G) T lymphoblasts expressing Lifeact-GFP were imaged live while interacting with coverslips coated with anti-CD3+ ICAM-1, analyzed as in C–E (1,180 measurements from 21 cells). Data in E and H represent means  $\pm$  SEM. Bars, 5  $\mu$ m.

had even more profound effects. Normalization to total LFA-1, however, revealed that there was no consistent difference in the proportion of IS-associated LFA-1 in the extended conformation after any treatment (Fig. 4 H). Labeling with m24 showed a modest but significant decrease in open LFA-1 at the IS after inhibition of myosin II with Y-27 and a similar trend with Bleb. A more profound diminution ( $\sim$ 60%) was observed after freezing the F-actin network (Fig. 4 F). In contrast to the extended conformation, loss of the open conformation in actin-arrested cells was profound, even after correction for changes in total LFA-1. Inhibition of myosin II alone resulted in a 20% decrease in the proportion of open LFA-1, whereas freezing the F-actin network resulted in a 42% decrease from control cells (Fig. 4 I).

Similar effects were observed in T cells responding to stimulatory bilayers. As in conjugates, we found that absolute levels of both the extended and open conformations decreased

upon arrest of F-actin flow (Fig. 5, B–E). On bilayers, these effects remained statistically significant after correction for diminished synaptic LFA-1 (Fig. 5, G and H). Some loss was also observed upon inhibition of myosin II alone, though whether this reached statistical significance was inhibitor-dependent. Collectively, these data show that myosin II contraction and F-actin dynamics are crucial for maintaining the high affinity conformation of LFA-1 at the IS.

#### F-actin dynamics regulate the organization of activated LFA-1

Freezing F-actin dynamics also affected the radial distribution of LFA-1 activation intermediates. The images in Figs. 4 and 5 reveal that the small number of activated LFA-1 molecules remaining at the IS became more randomly distributed. Analysis of radial intensity profiles showed that inhibition of myosin alone had little effect on the distribution of LFA-1 in any conformation,

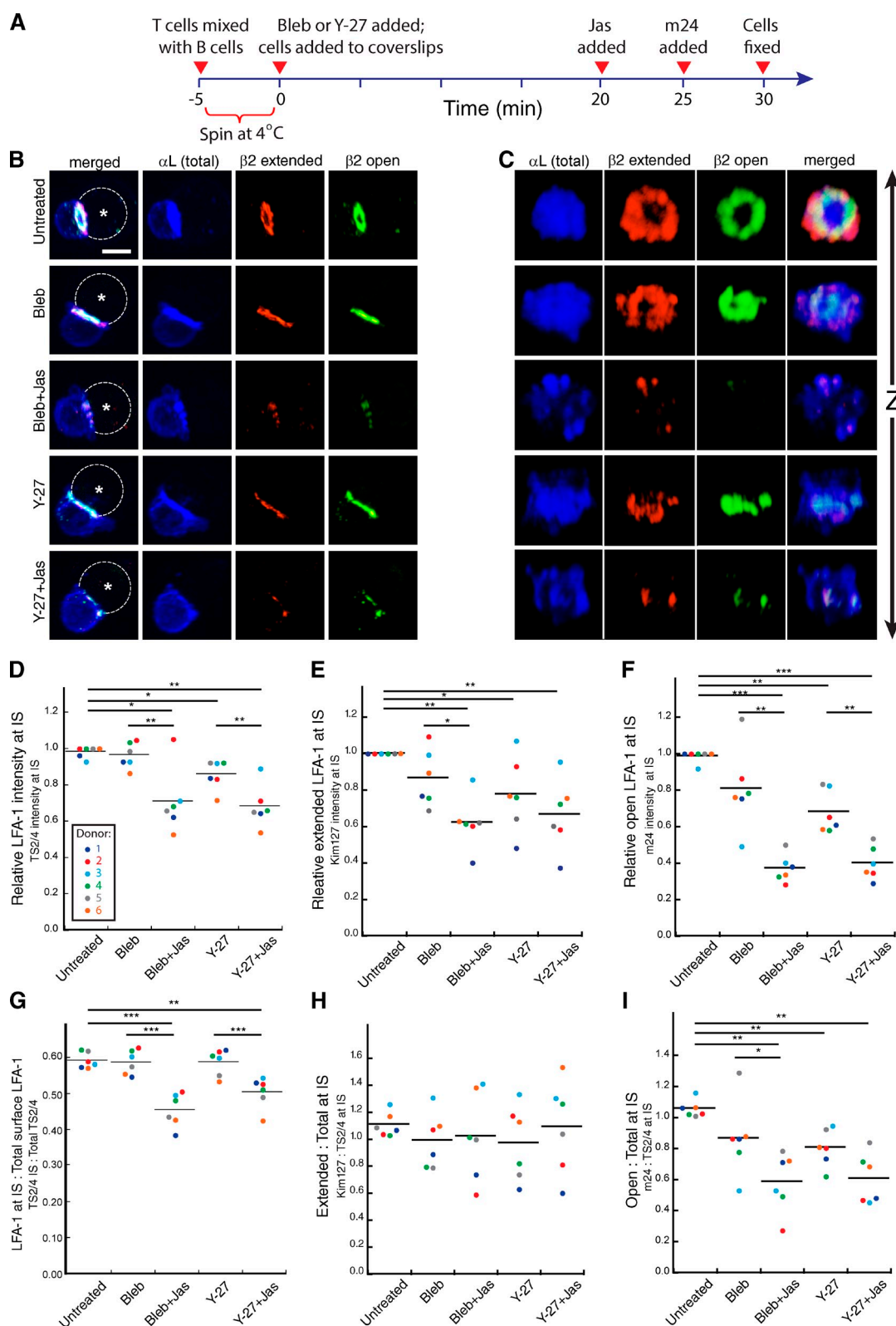


**Figure 4. Centripetal flow of the actomyosin network regulates valency and affinity of LFA-1.** (A) Ex vivo CD4<sup>+</sup> T cells were conjugated with SEE-pulsed Raji B cells and subjected to the indicated experimental paradigm. After fixation, cells were labeled with TS2/4 and Kim127. (B) Representative conjugates showing integrin localization and activation. The outline of the interacting B cell (asterisk) is indicated with a dotted line. Bar, 5  $\mu$ m. (C) Corresponding 3D rendering of the IS plane. (D–F) The effects of drug treatments on intensities of total (D), extended (E), and open (F) LFA-1 staining at the IS, each normalized to the untreated control. (G) The effects of drug treatments on maintenance of overall LFA-1 recruitment at the IS. (H and I) The effects of drug treatments on the proportion of LFA-1 in the extended (H) or open (I) conformations are shown based on signal intensity of conformation-specific antibodies, divided by the intensity of antibody recognizing total LFA-1. Data from six independent human donors (color coded in D) are shown; at least 30 conjugates were analyzed per condition for each donor. \*,  $P < 0.05$ ; \*\*,  $P < 0.01$ ; \*\*\*,  $P < 0.001$ .

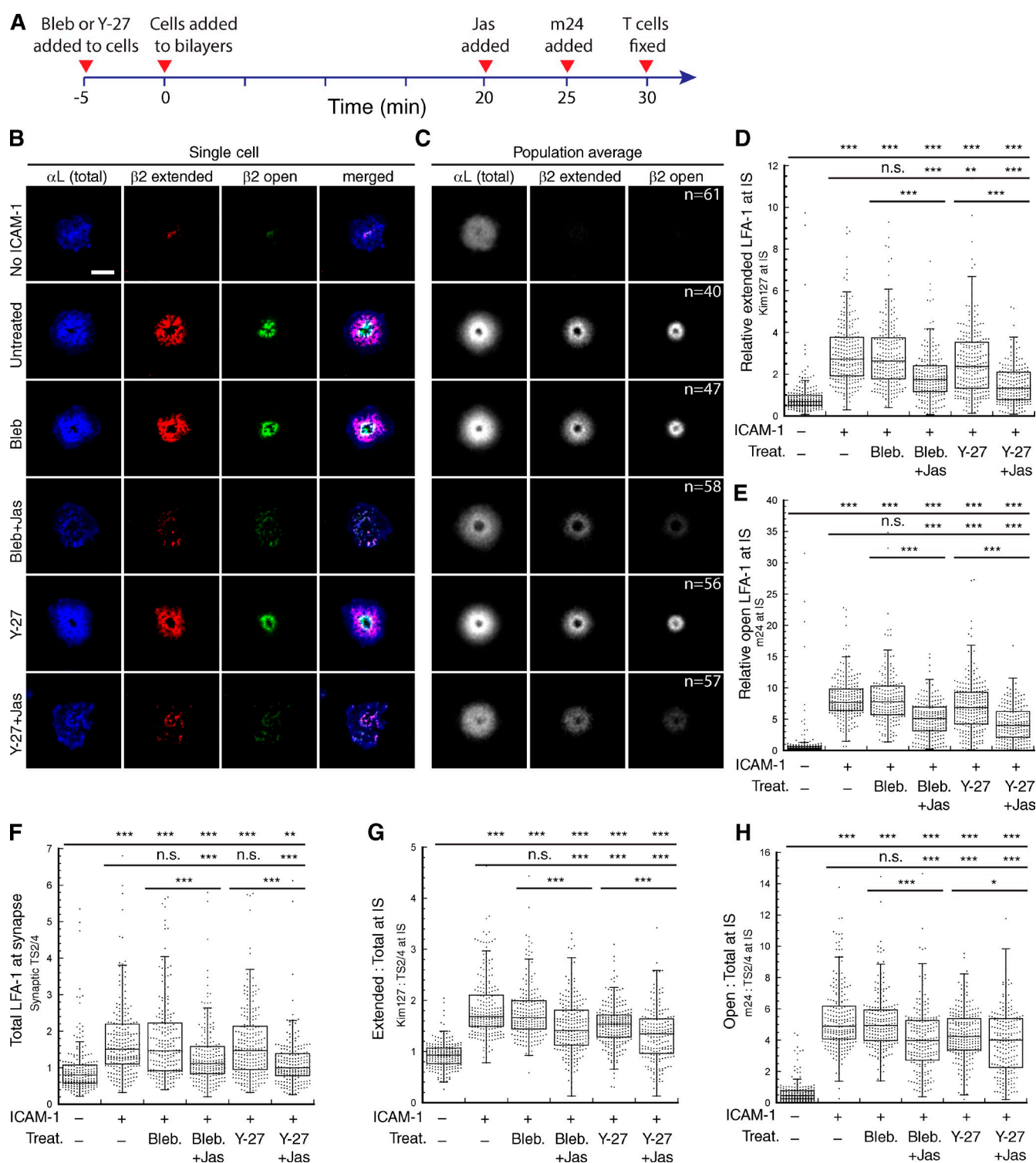


**Figure 5. F-actin dynamics regulate the organization of activated LFA-1.** (A) Ex vivo CD4<sup>+</sup> T cells spreading on bilayers coated with anti-CD3 in the presence or absence of ICAM-1 were subjected to the indicated experimental paradigm. After fixation, cells were labeled with TS2/4 and Kim127. (B) Representative synapses. Bar, 5  $\mu$ m. (C) Mean fluorescence intensity distributions for cell populations. (D–F) Cells were treated as in B, and the relative labeling intensity of LFA-1 in the extended conformation (D), open conformation (E), or total LFA-1 (F) was determined. (G and H) Ratio of extended (G) or open (H) conformations of LFA-1 to total LFA-1 at the IS. Data represent 130–250 cells per condition from a single representative donor;  $n = 3$  donors. \*,  $P < 0.05$ ; \*\*,  $P < 0.01$ ; \*\*\*,  $P < 0.001$ .

whereas arrest of actin flow profoundly affected both the extended and the open conformations (Fig. S4). The most dramatic change was the near complete loss of the peak of open

LFA-1. Collectively, these data demonstrate that the concentric pattern of LFA-1 activation intermediates is maintained by ongoing F-actin flow.



### Coengagement of $\beta 1$ integrins slows the F-actin network and attenuates LFA-1 activation

To complement these pharmacological studies, we sought a more physiological context in which T cell actin flow could be perturbed. In Jurkat T cells, it was previously shown that coengagement of VLA-4 ( $\alpha 4\beta 1$  integrin) with TCR slows actin flow at the IS (Nguyen et al., 2008). We therefore asked if ligation of VLA-4 has the same effect on primary T cells in the context of LFA-1 coengagement. T cells spreading on coverslips coated with a combination of anti-CD3, ICAM-1, and vascular cell adhesion molecule 1 (VCAM-1) spread to about the same extent as cells spreading on anti-CD3+ ICAM-1 alone (unpublished data). Actin flow rates reached  $60 \pm 35$  nm/s at the periphery of the IS, with a sixfold decrease in rate near the IS center (Fig. 6, A–C; and Video 7). Within the outer 40% of the IS radius where most F-actin dynamics occur, the flow rates were significantly lower than in cells spreading on anti-CD3+ ICAM-1 (Fig. S5). Correlating with slower actin rates, VCAM-1 coligation resulted in a 34% decrease in the total levels of open LFA-1 and a 20% decrease in the proportion of molecules in this conformation (Fig. 6 D). This effect is probably not caused by competition between  $\beta 1$  and  $\beta 2$  integrins for adaptor molecules involved in inside-out signaling because the proportion of LFA-1 molecules in the extended conformation actually increased upon  $\beta 1$  integrin engagement. Thus, we conclude that  $\beta 1$  integrin engagement modulates  $\beta 2$  integrin affinity maturation by slowing the flow of the actin network. This result also demonstrates that the actin network can serve as a mechanical link between distinct integrins and possibly between integrins and other cell surface receptors.

### Optimal LFA-1-ICAM-1 interactions require ongoing actin flow

A previous study using the planar bilayer system showed that depolymerization of actin filaments leads to loss of ICAM-1 recruitment and organization at the IS (Varma et al., 2006). Because we found that arresting actin flow leads to loss of the high affinity conformation of LFA-1, we wondered what impact this has on ICAM-1 binding. We therefore used planar bilayers containing fluorescent ICAM-1 in conjunction with conformation-specific antibodies and pharmacological inhibition of actin dynamics. As shown in Fig. 7 (A–C), inhibition of F-actin flow, but not inhibition of myosin II alone, caused a loss of ICAM-1 accumulation in the pSMAC region. As a second measure of ICAM-1 release, we labeled cells after fixation with TS1/22, an antibody that competes for ICAM-1 binding to the  $\alpha I$  domain of LFA-1, which should detect only unbound LFA-1 molecules. The proportion of LFA-1 molecules that bound TS1/22 was increased after arrest of actin flow (Fig. 7 D), again showing that optimal LFA-1-ICAM-1 interactions require ongoing actin flow rather than the presence of an immobile F-actin scaffold.

### LFA-1 activation requires a polarized TCR stimulus and immobilized ICAM-1

We were surprised to find significant levels of high affinity LFA-1 in T cells stimulated by anti-CD3 alone (Fig. 3 B)

given a previous study showing that TCR stimulation is insufficient to induce this conformational change (Schürpf and Springer, 2011). Importantly, whereas the earlier study used soluble stimuli, we delivered the TCR stimulus on planar surfaces. The architecture of the spreading T cell allows concerted F-actin flow, which could exert force on the cytoplasmic tail of LFA-1. In support of this idea, we found that soluble cross-linking of the TCR resulted in no cell spreading and no induction of the open conformation of LFA-1 (Fig. 8, A–C). In contrast, TCR cross-linking on a planar glass surface induced cell spreading and increased the proportion of extended-open LFA-1, even in the absence of ligand. As seen in Fig. 3 B, the activated LFA-1 was localized at the very center of the IS, consistent with the idea that actin flow shuttles the unbound integrin toward the IS center.

Using the same experimental system, we tested the mechanisms through which ICAM-1 binding promotes LFA-1 conformational change. Two nonexclusive possibilities exist: (1) an induced fit mechanism whereby ICAM-1 binding results in direct conformational change of LFA-1 and (2) a tension-based mechanism in which ICAM-1 opposes lateral movement of LFA-1, thereby contributing to force-dependent conformational change. To differentiate between these mechanisms, we delivered a TCR stimulus on planar surfaces and provided various LFA-1 stimuli. To test the contribution of induced fit in the absence of tension, soluble ICAM-1 (1  $\mu$ g/ml) was added. This condition did not lead to increased T cell spreading or LFA-1 activation and did not alter LFA-1 distribution at the IS (Fig. 8, A–C). To ask if tension is sufficient to increase LFA-1 activation, we added the monoclonal antibody TS1/22 to the stimulatory coverslips. This antibody binds the ICAM-1 binding site of the  $\alpha I$  domain in all LFA-1 conformations (Schürpf and Springer, 2011) and should therefore mimic tension induced by binding to immobilized ICAM-1 without the induced fit component. Engagement of LFA-1 by TS1/22 resulted in increased cell spreading, but did not increase the proportion of LFA-1 in the open conformation (Fig. 8, B and C). Interestingly, TS1/22 caused existing open LFA-1 to form a peripheral ring similar to that seen in the presence of immobile ICAM-1 (Fig. 8 A). Finally, to test the combined effect of induced fit and tension, cells were stimulated with immobilized ICAM-1. This condition resulted in increased cell spreading and LFA-1 redistribution similar to that seen with TS1/22. In addition, these cells showed a dramatic increase in the proportion of LFA-1 in the open conformation. Our finding that ICAM-1 immobilization is required to induce LFA-1 conformational change is consistent with previous work from Feigelson et al. (2010), though that study did not address the question of tension versus induced fit. We conclude that although tension on LFA-1 can promote T cell spreading and concentric organization, a combination of induced fit and tension is needed to support adoption of the open conformation. Finally, although the induced fit mechanism is sufficient to support conformational change of purified integrin ectodomains (Zhu et al., 2013) and at high soluble ligand densities (Dustin, 1998), this mechanism is not likely to play a large role at physiological ligand concentrations.

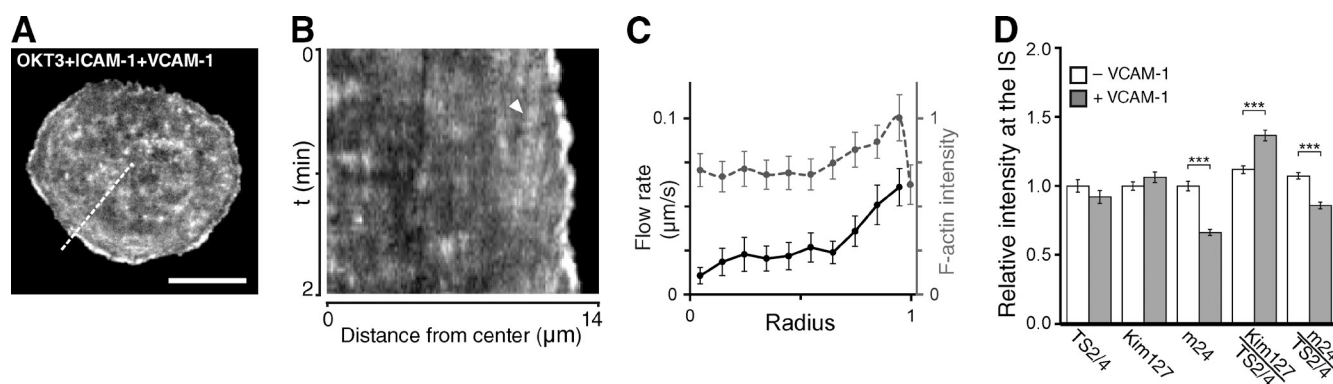


**Figure 6. Coengagement of VLA-4 slows F-actin flow and attenuates LFA-1 activation.** (A and B) T lymphoblasts expressing Lifeact-GFP were imaged while interacting with coverslips coated with anti-CD3, ICAM-1, and VCAM-1. (A) Single time point of a responding cell, and (B) corresponding kymograph of F-actin dynamics generated along the dashed line in A. Bar, 10  $\mu$ m. Arrowhead in B indicates a mobile fiducial mark. (C) Kymographic analysis of F-actin dynamics (817 measurements from 11 cells) superimposed with the normalized radial distribution of F-actin intensity in the same cells. Data represent mean  $\pm$  SEM. (D) T cells spreading on coverslips coated with anti-CD3 and ICAM-1 +/- VCAM-1 were labeled with the indicated antibodies and analyzed for fluorescence intensity in the IS plane. Results represent mean  $\pm$  SEM from one of three independent experiments. \*\*\*,  $P < 0.001$ .

## Discussion

Our results establish that centripetal flow of the T cell actin cytoskeleton drives LFA-1 recruitment to and affinity maturation at the IS, greatly enhancing the overall avidity of T cell-APC adhesion. This process also organizes LFA-1 conformational intermediates into a concentric array at the IS. These findings provide direct evidence in favor of a mechanical model for LFA-1 activation in which force generated by actin flow acts as a necessary component of integrin regulation at the IS (Fig. 9).

We find that F-actin flow is required for the maintenance of LFA-1 organization and affinity regulation. Because this requirement was observed even in T cells responding to artificial stimulatory surfaces, we conclude that cell-intrinsic forces are sufficient to produce ectodomain changes associated with affinity maturation. Mechanical force and ligand binding are functionally intertwined and both are required for full LFA-1 affinity maturation. Indeed, we observe a concomitant loss of both high affinity LFA-1 and bound ligand upon inhibition of actin dynamics, indicating that maintenance of the high affinity ligand-bound state requires ongoing tension. This behavior is consistent with known properties of catch bond molecular interactions (Thomas et al., 2008). Although our data show that physiological concentrations of surface-bound ligand are insufficient to maintain full LFA-1 activation in the absence of actin flow, it is known that ICAM-1 can, at high concentrations, induce LFA-1 conformational change (Dustin, 1998). In keeping with this, we find that ligand binding clearly enhances LFA-1 activation, and induced fit probably accounts for the residual levels of open LFA-1 we observe upon arrest of actin flow.

Our data indicate that regulation of LFA-1 conformational change occurs at several steps (Fig. 9 B). First, T cell spreading, and possibly actin polymerization and retrograde flow, drives the equilibrium toward the high affinity conformation in the absence of integrin ligand. Second, binding to immobilized ICAM-1 stabilizes the conformational change by opposing forces exerted on LFA-1 by the T cell cytoskeleton, as well as by induced fit, driving the equilibrium further toward the high affinity

conformation. At the same time, interplay between T cell actin forces and ligand-dependent retention of LFA-1 organizes active LFA-1 into concentric rings. The organization of these rings varies with the stimulatory surface, as this alters both ligand mobility and actin network behavior.

Exactly how actin flow works to organize LFA-1 at the IS is not clear. We did not observe direct colocalization of LFA-1 conformational intermediates with F-actin or myosin IIA. It seems likely that nascent LFA-1-ICAM-1 complexes originate in the F-actin-rich periphery and undergo flow-dependent coalescence (Kaizuka et al., 2007). Because high affinity LFA-1 molecules are tightly linked to the actin cytoskeleton (Cairo et al., 2006), this conformation may be selectively delivered to the inner region of the IS by F-actin flow. The alternative possibility is that actin flow activates LFA-1 as it is being shuttled to the cSMAC. Both of these models are consistent with our observation that active LFA-1 is shifted toward the periphery under conditions of low ICAM-1 mobility. Finally, because the cSMAC region is also associated with endocytosis, secretion, and exosome release (Griffiths et al., 2010), membrane trafficking events may also play a role. In particular, mechanical activation of LFA-1 may be associated with membrane internalization, a process that would involve pN-scale forces orthogonal to the cell membrane. Distinguishing among these models will require the development of biosensors that can measure LFA-1 conformational change in real time. Another open question is what defines the inner boundary where open LFA-1 accumulates. LFA-1 may be deposited in this region as a result of slowing and disassembly of the actin network. Alternatively, LFA-1 may be excluded based on molecular crowding or kinetic segregation (Davis and van der Merwe, 2006; Kaizuka et al., 2007; Hartman et al., 2009). Finally, exclusion could be mediated by membrane trafficking events because this area of the IS is associated with endocytosis and protein degradation as well as extrusion of TCR-enriched extracellular vesicles (Vardhana et al., 2010; Choudhuri et al., 2014).

The relative contribution of LFA-1 valency and affinity to the formation and maintenance of T cell-APC contacts has been

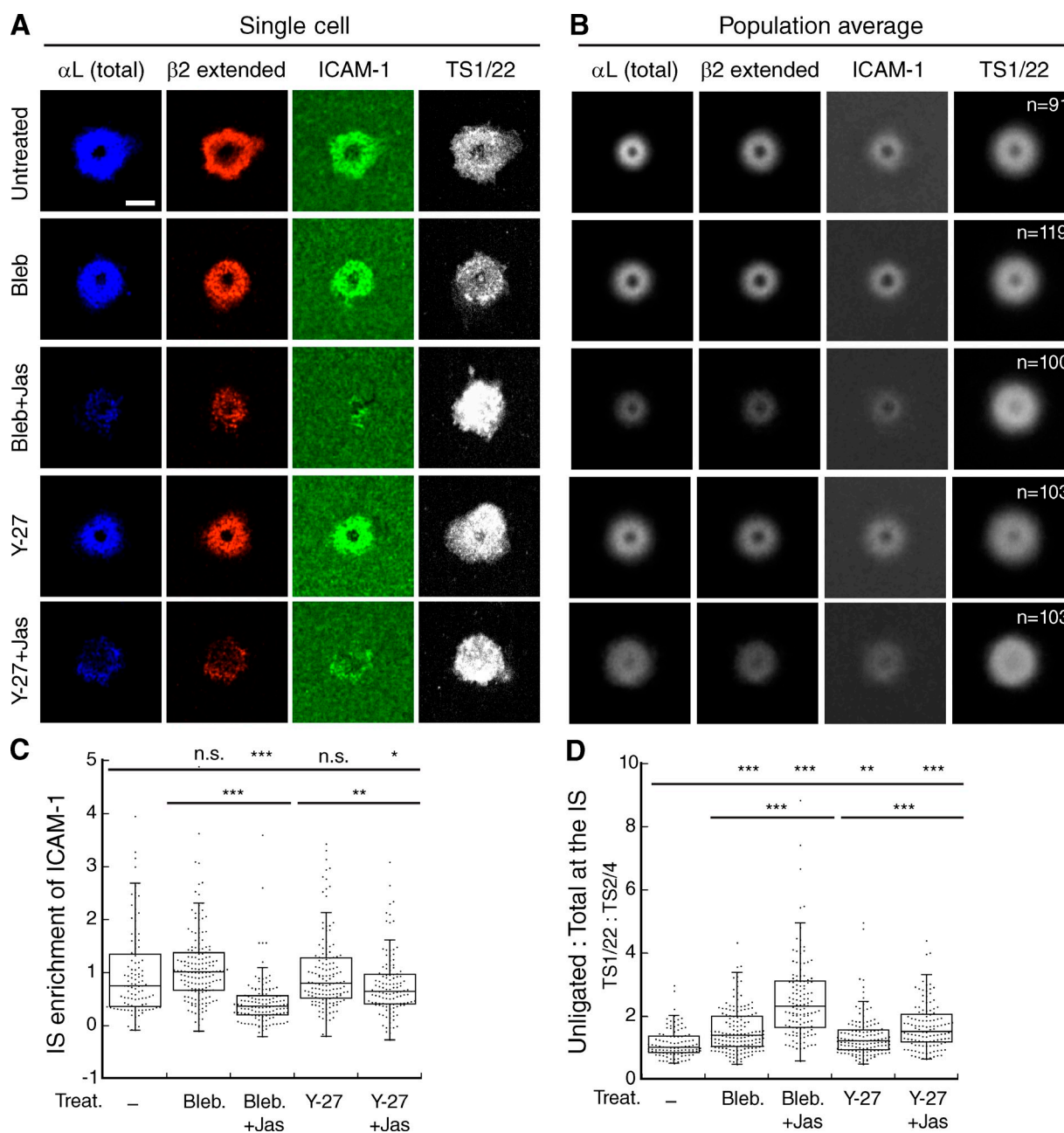


**Figure 7. LFA-1-ICAM-1 interactions are maintained by ongoing F-actin dynamics.** Ex vivo CD4<sup>+</sup> T cells were treated with inhibitors as in Fig. 5 and allowed to spread on planar bilayers functionalized with anti-CD3 and Alexa Fluor 488-labeled ICAM-1. Cells were then fixed and stained with TS2/4, Kim127, and TS1/22. Bar, 5  $\mu$ m. Representative cells (A) and population average projections (B). (C) Quantification of ICAM-1 enrichment under the cell after subtracting background levels of ICAM-1. Values are normalized to the untreated control. (D) Ratio of unligated to total LFA-1 defined by staining with TS1/22 and TS2/4, respectively. Data represent 100–150 cells per condition from a single representative donor;  $n = 3$  donors. \*,  $P < 0.05$ ; \*\*,  $P < 0.01$ ; \*\*\*,  $P < 0.001$ .

a subject of ongoing debate (Carman and Springer, 2003; Kim et al., 2004). We show here that T cell actin flow drives both aspects of avidity modulation. Although flow is required to maintain the high affinity conformation of LFA-1 independent of changes in valency, it also maintains overall accumulation of LFA-1 at the IS (Fig. 9 A). The combination of these two effects can be measured as the total amount of open LFA-1 at the IS, a value that drops by 60% after inhibition of actin flow.

In the course of these studies we found that engagement of different integrins by immobilized ligands has distinct effects

on F-actin dynamics at the IS. In Jurkat T cells, VLA-4 binding to VCAM-1, but not LFA-1 binding to ICAM-1, brings F-actin flow nearly to a halt (Nguyen et al., 2008; unpublished data). In primary T cells, engagement of LFA-1 induced very modest slowing of the actin network, but coengagement of LFA-1 and VLA-4 induced significant slowing. The underlying mechanisms remain to be identified; one plausible idea is that the  $\beta$ 1 and  $\beta$ 2 chains differ in their interactions with actin-binding adapter molecules. Consistent with the observed slowing of the actin network, we observed diminished LFA-1 activation with the



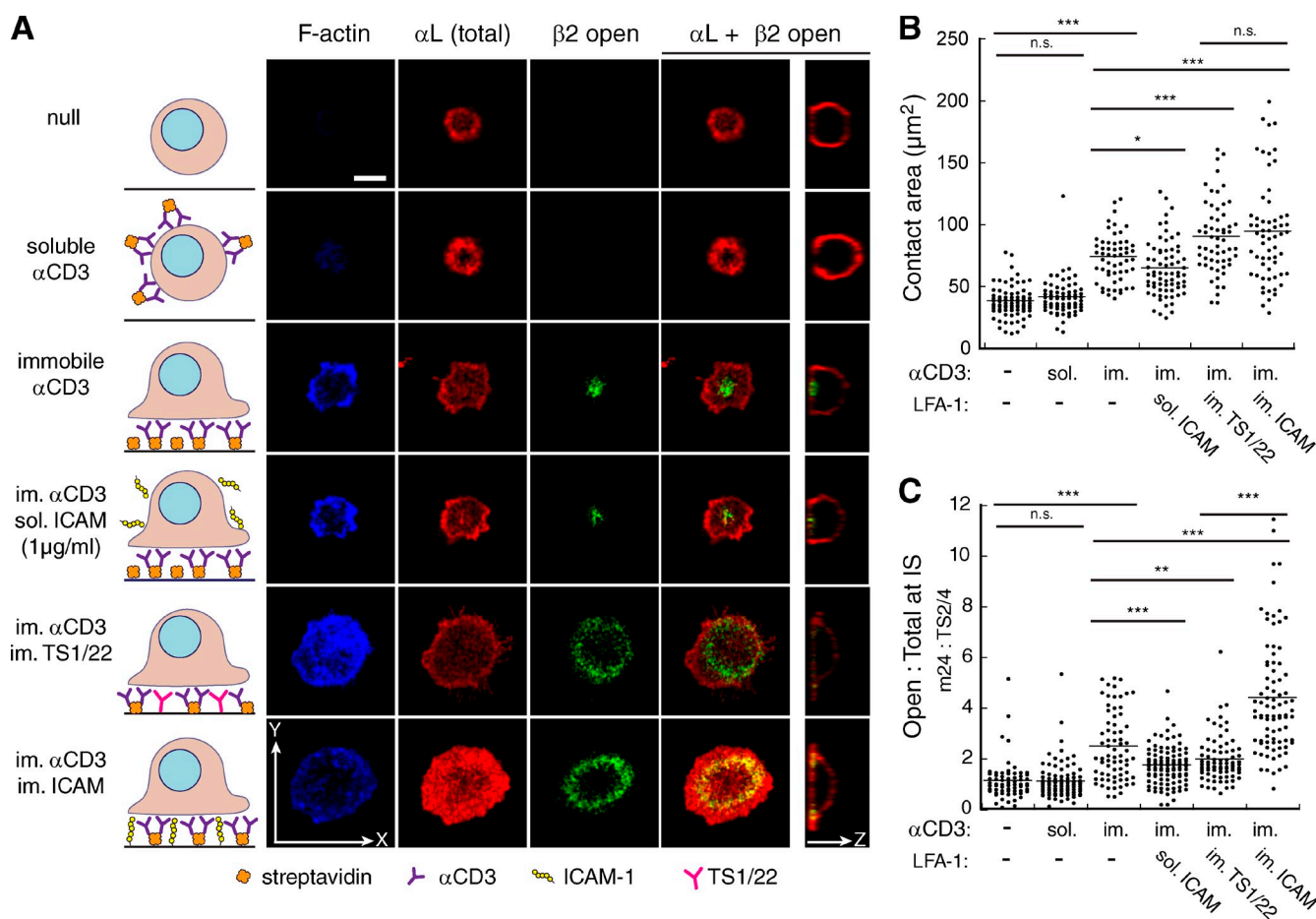


**Figure 8. LFA-1 activation requires a polarized TCR stimulus and immobilized ICAM-1.** (A) T cells were either left untreated or incubated on ice with biotinylated anti-CD3, and then stimulated at 37°C with either soluble streptavidin (soluble  $\alpha$ CD3) or coverslip-adsorbed streptavidin (immobile  $\alpha$ CD3). Some cells were concomitantly stimulated with either soluble ICAM-1 (sol. ICAM), coverslip-adsorbed TS1/22 (im. TS1/22), or coverslip-adsorbed ICAM-1 (im. ICAM). Images show single confocal planes near the contact site. (B) Contact area of cells from A. (C) Proportion of LFA-1 in the open conformation on different stimulatory surfaces. Data represent at least 70 cells per condition from a single representative donor;  $n = 3$  donors. \*,  $P < 0.05$ ; \*\*,  $P < 0.01$ ; \*\*\*,  $P < 0.001$ .

addition of VCAM-1. This has important functional implications because up-regulation of VLA-4 during T cell activation could effectively down-regulate LFA-1-dependent interactions.

A recurring conundrum in mechanobiology is the difficulty in separating force-dependent processes from conventional signaling events. Because the inhibitor cocktail used here to arrest actin dynamics also perturbs sustained  $\text{Ca}^{2+}$  elevation (but not early tyrosine phosphorylation events) downstream of the TCR (Babich et al., 2012), it is possible that the observed loss of LFA-1 activation results from impaired conventional signaling rather than cessation of force. Several pieces of data support our interpretation that force plays a key role. First, inside-out signaling is traditionally thought to culminate with talin binding and induction of the extended conformation, but we find that inhibiting actin dynamics has the most profound and consistent effect on transition to the open conformation. Second, slowing the actin network by engaging VLA-4 also diminishes LFA-1 conformational change, even though it actually enhances TCR signaling (Nguyen et al., 2008). Finally, in cells treated with soluble ICAM-1, TCR signaling and actin flow are intact, yet LFA-1 conformational change does not occur in the absence of tension generated by immobilized ligand.

Our data do not preclude cytoskeletal regulation of other molecules involved in LFA-1 activation. In focal adhesions, talin and vinculin both depend on force transmission for proper function. Actin-dependent stretching of talin reveals cryptic binding sites for vinculin, which creates additional F-actin linkages (Margadant et al., 2011; Ciobanaru et al., 2013; Hirata et al., 2014). In T cells, vinculin is recruited to the IS and is required for talin recruitment and conjugate formation (Nolz et al., 2007). Thus, talin and vinculin could enhance cytoskeletal anchorage of LFA-1 under conditions where F-actin flow generates tension. This could explain our observation that open LFA-1 becomes homogeneously distributed upon inhibition of F-actin flow; when vinculin dissociates, talin-bound LFA-1 could diffuse more readily.

In addition to maintaining adhesive contacts, integrins act as traditional signaling receptors in a process termed outside-in signaling. LFA-1 engagement induces formation of signaling microclusters (Baker et al., 2009; Wang et al., 2009) and leads to activation of multiple signaling intermediates (Tabassam et al., 1999; Perez et al., 2003; Li et al., 2009; Varga et al., 2010). Indeed, LFA-1 can be considered a costimulatory molecule in that its coengagement with TCR lowers the threshold for T cell



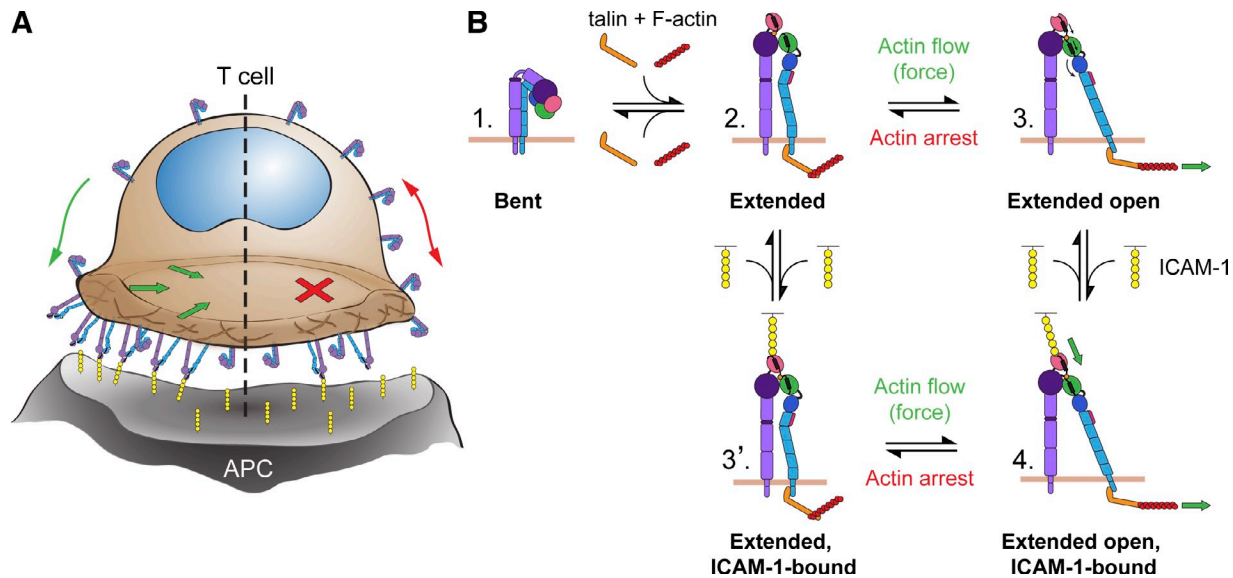


**Figure 9. Model of LFA-1 activation at the IS.** (A) Actin-dependent regulation of LFA-1 valency. Ongoing F-actin flow (left) in T cells responding to a polarized TCR stimulus drives activation of LFA-1 at the IS. Activated LFA-1 then binds ICAM-1, leading to synaptic enrichment. Arrested F-actin dynamics (right) abrogates activation of LFA-1, allowing passive diffusion of unligated LFA-1 away from the IS. (B) Actin-dependent regulation of LFA-1 affinity. (1) Inactive LFA-1 exists in a bent conformation on the T cell surface. (2) Inside-out signaling events downstream of TCR engagement lead to recruitment of talin and F-actin to the integrin  $\beta$  tail. This allows for the segregation of the  $\alpha$  and  $\beta$  tails and the unbending of LFA-1 to yield the extended conformation. (3) F-actin flow generates tensile force on the LFA-1  $\beta$  tail (green arrow), facilitating further tail separation and resulting in swingout of the hybrid domain and induction of the open (high affinity) form of LFA-1. (4) The open  $\alpha$  domain primes the molecule for binding of ICAM-1, which through induced fit and tension-based mechanisms (green arrows) stabilizes LFA-1 in the high affinity, ligand-bound conformation. Alternatively, LFA-1 affinity maturation can proceed through an ICAM-1-bound, extended conformation (3') in which ICAM-1 weakly interacts with LFA-1 and induces the open head domain before application of force; force then stabilizes this interaction. After loss of force on the  $\beta$  chain, ligand unbinding may preferentially occur through the 3' step, in which there is no stabilization of the open  $\alpha$  domain and therefore much lower affinity for ICAM-1. Alternatively, in the absence of force, LFA-1 does not undergo the priming step to the unligated, open conformation. Regular turnover of LFA-1–ICAM-1 complexes would then lead to loss of bound ICAM-1.

activation (Perez et al., 2003; Suzuki et al., 2007). The relationship between conformational change and outside-in signaling for LFA-1 has not been rigorously addressed, but outside-in signaling by other integrins is associated with their high affinity forms (Zhu et al., 2007; Lefort et al., 2009). Assuming that the high affinity conformation of LFA-1 also represents the signaling competent pool, actin flow should promote LFA-1 signaling and costimulation. Further analysis will be needed to test this directly.

Our data support a model in which ICAM-1 mobility is an important parameter for LFA-1 activation. Low mobility ICAM-1 would provide greater resistance to forces exerted on LFA-1 by the T cell actin cytoskeleton and should therefore be better at inducing conformational change. In support of this idea, artificially increasing ICAM-1 mobility in target cells diminishes conjugate formation and granule polarization by natural killer cells (Gross et al., 2010). This raises the intriguing possibility that APCs could regulate lateral mobility of integrin ligands to modulate T cell activation. Indeed, in the accompanying paper, we show that dendritic cells control ICAM-1 mobility through regulated cytoskeletal changes and that manipulation of ICAM-1 mobility modulates LFA-1 conformational change and alters the antigen threshold for T cell adhesion and priming (see Comrie et al. in this issue). Together, these two studies show that the T cell and dendritic cell cytoskeletal networks work in concert to regulate adhesion and signaling at the IS.

In conclusion, our results provide strong evidence that centripetal flow of the T cell F-actin network provides mechanical force contributing to LFA-1 activation and ICAM-1 engagement at the IS. We propose that F-actin flow drives a positive feedback loop for IS-associated signaling events, whereby early TCR signals induce robust actin flow, which in turn increases signaling through mechanosensitive molecules like LFA-1.

## Materials and methods

### General reagents and antibodies

Unless otherwise noted, chemicals were purchased from Sigma-Aldrich. Y-27 and (–)-Bleb were purchased from EMD Millipore. Jasplakinolide, Alexa Fluor 647–streptavidin, Alexa Fluor 594–phalloidin, and antibody labeling kits for Alexa Fluor 488 and 594 were purchased from Life Technologies. Streptavidin was purchased from Jackson ImmunoResearch Laboratories, Inc. CF405M phalloidin was purchased from Biotium. DyLight 650 labeling kits were purchased from Thermo Fisher Scientific. Mouse anti-CD43 antibody (clone 1G10) was purchased from BD. Goat polyclonal antibody against talin was purchased from Santa Cruz Biotechnology, Inc. Rabbit polyclonal antibody against myosin IIA heavy chain was purchased from Covance. Leaf-purified mouse anti-CD3 (OKT3; BioLegend) and biotinylated OKT3 (eBioscience) were used for T cell stimulation. Biotinylated mouse anti-CD3 antibody SK7 (BioLegend) was used for immunolabeling of fixed cells. Human ICAM-1-Fc and VCAM-1-Fc chimeras were purchased from R&D Systems. As a source of mouse ICAM-1, we used 293T cells stably transfected with a pBabe<sup>+</sup>CMV-Puro vector encoding the extracellular domain (amino acids 1–485) of mouse ICAM-1 with a C-terminal 6 $\times$  His tag (provided by E. Long, National Institutes of Health, Bethesda, MD). ICAM-1–His was purified from these cells as previously described (March and Long, 2011). In brief, cells were grown for 5 d in serum-free medium

and protein was isolated from supernatants by passage over Ni-NTA column and elution with 500 mM imidazole in PBS.

#### LFA-1 conformation-specific antibodies

Mouse monoclonal antibodies TS2/4 (anti-CD11a), TS1/22 (anti-CD11a), and Kim127 (anti-CD18) were harvested from hybridomas (ATCC). TS1/22 was also purchased from Thermo Fisher Scientific. Mouse monoclonal antibody m24 (anti-CD18) was purchased from Abcam. TS2/4 recognizes an epitope on the  $\beta$  propeller domain of CD11a ( $\alpha$ L) only in the assembled  $\alpha\beta$  heterodimer (Huang and Springer, 1997) and binds in an activation-independent manner (Chen et al., 2006). TS1/22 binds to the  $\alpha$ L domain of CD11a and competes directly for ICAM-1 binding. It can therefore be used to report on unbound LFA-1 (Schürpf and Springer, 2011). Kim127 binds to an epitope within the EGF2 domain of CD18 ( $\beta$ 2) that is hidden in bent, inactive integrins and exposed upon integrin extension and activation. Kim127 therefore reports on the extended and open conformations (Lu et al., 2001; Chen et al., 2006). Because Kim127 is an activating antibody, care was taken to use it only after fixation. m24 binds the activated 1 domain of CD18 ( $\beta$ 2) after hybrid domain swingout, and therefore reports on the high affinity extended-open conformation of LFA-1 (Dransfield and Hogg, 1989; Chen et al., 2006; Chen et al., 2010; Schürpf and Springer, 2011). The epitope bound by m24 is sensitive to aldehyde fixation, necessitating prefixation labeling. On its own, m24 does not induce LFA-1 conformational change, though it can stabilize the ICAM-1 bound open conformation (Smith et al., 2005). Thus, care was taken to minimize labeling times and antibody concentration. TS2/4 was directly conjugated to Dylight 650, Kim127 was conjugated to Alexa Fluor 594, and m24 was conjugated to Alexa Fluor 488, all according to the manufacturers' protocols. Functionality of antibodies was verified by flow cytometry on unstimulated T cells or cells stimulated with  $Mn^{2+}$ .

#### Cell culture

Unless otherwise indicated, T cells refers to ex vivo human peripheral blood CD4<sup>+</sup> T cells. Human peripheral blood CD4<sup>+</sup> T cells or CD8<sup>+</sup> T cells were obtained from the University of Pennsylvania's Human Immunology Core under an Institutional Review Board–approved protocol. In experiments using ex vivo cells, T cells were used within 3 h of purification. Alternatively, T lymphoblasts were generated by activation with human T-Activator CD3/CD28 magnetic beads (Dynabeads; Life Technologies) in RPMI (Invitrogen) supplemented with 10% FBS (Atlanta Biologicals), 1% GlutaMAX (Invitrogen), 1% Pen/Strep, and 50 U/ml of human rIL-2 (obtained through the AIDS Research and Reference Reagent Program, Division of AIDS, National Institute of Allergy and Infectious Diseases, National Institutes of Health, from M. Gately, Roche, Nutley, NJ). T lymphoblasts were cultured in a humidified 37°C incubator with 5% CO<sub>2</sub>. Beads were magnetically removed on day 6 after initial stimulation and cells were then cultured for an additional day in the absence of IL-2. The human B cell line Raji was cultured in RPMI with 10% FBS, 1% GlutaMAX, and 1% Pen/Strep. 293T cells (ATCC) were grown in DMEM (Invitrogen) supplemented with 10 mM Hepes, 10% FBS, 1% GlutaMAX, 1% Pen/Strep, and 1% NEAA (Invitrogen).

#### Plasmids and transduction

Lentiviral packaging constructs psPAX2 and PDM2.G as well as Gateway donor vector pDONR221 and destination vector pLX301 were all gifts of N. Hacohen, Broad Institute, Cambridge, MA. cDNA encoding F-actin-binding peptide Lifeact (amino acids 1–17 of the *Saccharomyces cerevisiae* protein Abp140) tagged on the C terminus with EGFP (Riedl et al., 2008) was subcloned into pDONR221 and subsequently into pLX301 using Gateway Technology. To generate recombinant lentivirus,  $1.8 \times 10^6$  293T cells were seeded in 15-cm plates the day before transfection, and then cotransfected using the calcium phosphate method with 48  $\mu$ g of each DNA of interest (all in pLX301), together with 36.3  $\mu$ g of psPAX2 and 12.1  $\mu$ g of pMD2.G. Media was exchanged after 18 h with fresh media. Supernatant was harvested 24 h later and was immediately used to transduce T cells. T cells were transduced by spin infection with lentivirus on day 3 after activation. Lentivirus and 8  $\mu$ g/ml Polybrene (Sigma-Aldrich) were added along with  $2 \times 10^6$  T cells to the wells of a 6-well culture plate and centrifuged at 2,000 rpm and 37°C for 2 h. Lentivirus-containing media was then replaced with T cell culture media, and the cultures were maintained as described in Cell culture.

#### Preparation of supported planar lipid bilayers

Lipids [DOPC, DSPe-PEG2000-biotin, and DOGS-NTA nickel salt; Avanti Polar Lipids, Inc.] were reconstituted in chloroform at 89.9:0.1:10 mol%, respectively. The mixture was then dried under a gentle stream of air and

desiccated in a vacuum chamber for 1 h. The dried lipid cake was hydrated in PBS, sonicated using a tabletop sonicator (Branson) for 15 min to generate multilamellar vesicles, and passed through a 50-nm pore membrane using a mini-extruder (Avanti Polar Lipids, Inc.). The resulting small unilamellar vesicles were stored at 4°C and used within 2–3 wk.

25  $\times$  75-mm glass slides (#1.5; Thermo Fisher Scientific) were cleaned for 15 min using Piranha solution (3:1 ratio of sulfuric acid and 30% hydrogen peroxide; Dustin et al., 2007) and then washed thoroughly with distilled water. Slides were then air dried and adhered to Sticky-Slide V1<sup>0.4</sup> Luer closed chambers (Ibidi). Small unilamellar vesicles in PBS were added to the chambers to cover the exposed glass surface for 15 min. After thorough rinsing with PBS, the chambers were incubated with ICAM-1 6 $\times$  His (0.3  $\mu$ g/ml unless stated otherwise), followed by 1  $\mu$ g/ml streptavidin, or Alexa Fluor 647–streptavidin for 15 min, and then thoroughly rinsed again with PBS and incubated with 1  $\mu$ g/ml OKT3-biotin for 15 min. Where indicated, bilayers were incubated with 0.3  $\mu$ g/ml of Alexa Fluor 488– or 594–labeled ICAM-1 in place of unlabeled ICAM-1. Chambers were rinsed and left in HBS supplemented with  $Ca^{2+}/Mg^{2+}$ , 1% BSA, and 2 mg/ml D-glucose. Lipid bilayers were used for imaging studies on the same day.

#### Preparation of stimulatory glass surfaces

For fixed cell studies, 12-mm coverslips (#1.0; Bellco) were coated with 10  $\mu$ g/ml OKT3 for 2 h at 37°C or overnight at 4°C, washed with PBS, and incubated with 1  $\mu$ g/ml ICAM-1 6 $\times$  His or ICAM-1 Fc. Where indicated, coverslips were subsequently incubated with VCAM-1 at 1  $\mu$ g/ml for 2 h at 37°C. Glass surfaces for live cell imaging studies were prepared similarly, except that 8-well Lab-Tek II chambered cover glasses (Thermo Fisher Scientific) were used.

#### Fluorescence microscopy

T cells were harvested and resuspended at  $5 \times 10^5$ /ml in L-15 medium for coverslip and conjugate experiments and at  $10^6$ /ml in HBS supplemented with  $Ca^{2+}/Mg^{2+}$ , 1% BSA, and 2 mg/ml D-glucose for lipid bilayer experiments. Coverslips or chambers were equilibrated at 37°C, and  $\sim 5.0 \times 10^4$  cells (for coverslips) or  $\sim 1.5 \times 10^5$  cells (for lipid bilayers) were allowed to interact with the surfaces for the indicated times. For T-B conjugates, Raji B cells were pulsed before interaction with T cells with 2  $\mu$ g/ml SEE (Toxin Technologies) for 1 h at 37°C and allowed to interact with T cells for 30 min. After stimulation, cells were fixed in 3% paraformaldehyde in PBS and quenched with 50 mM NH<sub>4</sub>Cl.

Cell surface LFA-1 and TCR were labeled before permeabilization, after which cells were permeabilized and blocked with 0.01% saponin and 0.25% fish skin gelatin in TBS, pH 7.4 (TSG). Cells were incubated for 40 min with primary antibodies in TSG, washed 3 $\times$  in TSG, and incubated with secondary antibodies in TSG for 40 min. Cells were then washed 3 $\times$  in TSG, once with 1% FBS in PBS and once with Milli-Q H<sub>2</sub>O, and mounted on slides with Mowiol mounting media (Sigma-Aldrich). Because the epitope recognized by m24 is destroyed by fixation, m24 antibody was added to live cells before fixation. Unless otherwise indicated, m24 labeling was restricted to 5 min at 1–2  $\mu$ g/ml. Kim127, TS2/4, and TS1/22 labeling was performed after fixation (and always before permeabilization) with Kim127 added first to minimize possible steric hindrance of the activation-dependent epitope.

To assess the role of TCR and LFA-1 ligand immobilization on the activation of LFA-1, ex vivo CD4<sup>+</sup> T cells were either left untreated or incubated with biotinylated OKT3 (10  $\mu$ g/ml) on ice for 10 min. Cells were then washed, warmed to 37°C in L-15 imaging medium, and stimulated with either soluble or surface-immobilized streptavidin on coverslips coated with  $\alpha$ CD43 (0.5  $\mu$ g/ml) and BSA (1 mg/ml) to allow binding without inducing nonspecific spreading. Some cells were also additionally stimulated with either soluble ICAM-1, coverslip-immobilized TS1/22, or coverslip-immobilized ICAM-1 (all at 1  $\mu$ g/ml). After 20 min of spreading, cells were fluorescently labeled with the indicated reagents as described in the previous paragraph.

All imaging was performed using a microscope (Axiovert 200; Carl Zeiss) equipped with a spinning disk confocal system (UltraView ERS6; PerkinElmer) and a 63 $\times$  planapo 1.4 NA objective. Images were collected using an Orca ER camera (Hamamatsu) and analyzed using Velocity 6.3 (PerkinElmer). For fixed cell imaging of T cell spreading on stimulatory planar surfaces, a single confocal plane was imaged at the contact interface. For T-B cell conjugates, whole conjugates were imaged as 10–12- $\mu$ m-thick z stacks, with planes spaced 0.25  $\mu$ m apart, and synapses were rendered in Volocity. 25–50 spread T cells or conjugates were selected per condition and used for further analysis. For live cell imaging, wells were covered

with 400  $\mu$ l of L-15 medium and equilibrated to 37°C on the microscope stage. Cells were harvested and resuspended in L-15 medium at  $2 \times 10^6$ /ml, and 5–10  $\mu$ l of cell suspension was added to the well. 0.5- $\mu$ m-thick z stacks consisting of three planes (0.25  $\mu$ m apart) were collected at the contact interface every 2 s for 2 min unless otherwise indicated. Stacks were displayed as maximum intensity projections.

### Image analysis

Kymographic analysis was performed essentially as described previously (Babich et al., 2012). In brief, movies of T cells expressing Lifeact-GFP were collected and analyzed in Volocity 6.3. A ray was struck from the center of the IS to the periphery, and vertical kymographs were generated. The flow rate of fiducial F-actin features was calculated based on the slope of deflection from the vertical direction. Instantaneous velocities were plotted as a function of the IS radius and grouped into ten equally spaced bins. In cases where a single actin feature traversed multiple bins, the instantaneous velocity of that feature was counted separately in each bin. For publication purposes, all kymographs were digitally enhanced using the Smart Sharpen filter in Photoshop (Adobe), with 150% amplification of local maxima within a 2-pixel radius.

Measurements of molecular distribution across the IS were done in two ways. The first method was based on mean intensity projections. For this, images of T cells were cropped to the same size, aligned based on the centroid for each cell, and imported as a stack into ImageJ 1.46r (National Institutes of Health). The stack of all cells was projected as a mean intensity image to generate a pattern of fluorescence distribution for the cell population, and the radial profile plug-in was used to obtain mean intensity values along the radius of the projected IS. Although this method is analytically powerful, it relies on the availability of a large number of images and works best when cell radii are relatively homogeneous in the population. Therefore, an alternate approach was sometimes used, based on normalizing cell radii to 1. This procedure was necessary for analysis of conjugates (Fig. 1) because the rendered images of the IS plane lack absolute length scales and for T lymphoblasts, which have a large variation of cell radii (Fig. 3). For this method, radial intensity values determined using the imageJ radial intensity plugin or individual line profiles from individual synapses were imported into Excel (Microsoft) and all radii were normalized to 1. Fluorescence intensity values based on percentage of maximum intensity in the population were binned according to their relative position along the normalized IS radius, and values within each bin were used to determine mean and standard error. Comparison of results from the two methods shows that they are generally interchangeable.

To assess IS area and total fluorescence intensity, Volocity software was used to identify T cell IS boundaries based on thresholds for total surface LFA-1 (TS2/4) or F-actin intensity (if TS2/4 staining was not available). IS area was calculated automatically by integrating the pixels within the identified objects. Total fluorescence intensity from the IS area was determined after background correction based on fluorescence from the unoccupied stimulatory surface, and values for control cells were then set to 1. To assess enrichment at the IS in conjugates, a region of interest was defined by eye for the IS and for the entire cell, and labeling intensity at the IS was divided by total cell surface labeling intensity for each cell. Because total integrin levels on the cell surface and at the IS were affected by pharmacological manipulations, the relative proportion of molecules undergoing conformational change was assessed by determining the total labeling intensity for conformation-specific antibodies (Kim127, TS1/22, or m24) and dividing this value by the total labeling intensity for all TS2/4-labeled LFA-1 molecules for each image. Note that this analysis cannot provide an absolute proportion of molecules in any given conformation, but it can be used to compare changes in relative proportions in response to experimental manipulations. ICAM-1 enrichment was determined by taking the mean ICAM-1 fluorescence intensity under the responding cell (cell boundaries were defined by TS2/4 localization) and subtracting the mean ICAM-1 fluorescence intensity of the bilayer away from sites of cell binding. The values were then normalized, with the mean response of the untreated control set to 1.

### Statistical analysis

Statistical analysis was performed using Excel. In individual experiments, statistical significance was determined using a two-tailed Student's *t* test for unpaired samples with equal variances. When comparing changes in populations of donors, a two-tailed Student's *t* test for paired samples was performed. Values 2 SDs from the mean were discounted as outliers. Where included, box and whisker plots are centered on the median, with upper and

lower quartile ranges. Outliers (determined as values that are  $>1.5\times$  the interquartile distance above the upper quartile or below the lower quartile) are shown.

### Online supplemental material

Fig. S1 shows analysis of LFA-1 activation intermediates, talin localization, and ICAM-1 binding. Fig. S2 shows that LFA-1 conformational change and synaptic patterns vary with ICAM-1 concentration. Fig. S3 shows that centripetal flow of the actomyosin network regulates valency and affinity of LFA-1b (data from a single donor). Fig. S4 shows that F-actin flow maintains the high-affinity conformation of LFA-1 and its localization at the IS. Fig. S5 shows that coengagement of integrin ligands modulates centripetal F-actin flow. Video 1 shows that LFA-1 activation intermediates are organized into a concentric array in T cell–B cell conjugates. Video 2 shows molecular dynamics in T lymphoblasts spreading on stimulatory bilayers. Video 3 shows an example of a T lymphoblast with no apparent cSMAC spreading on stimulatory bilayers. Video 4 shows tracking of F-actin dynamics in T cells spreading on stimulatory coverglasses. Video 5 shows F-actin dynamics in T lymphoblasts spreading on coverglasses coated with anti-CD3+/- ICAM-1. Video 6 shows that F-actin dynamics persist in human T cells treated with myosin II inhibitors but cease completely after subsequent addition of jasplakinolide. Video 7 shows that F-actin flow is slowed by the addition of immobilized VCAM-1. Online supplemental material is available at <http://www.jcb.org/cgi/content/full/jcb.201406121/DC1>.

We thank members of the Burkhardt laboratory, Tim Springer and Michael March for helpful discussions, Sudha Kumari and Michael Dustin for help with planar bilayers, Minsoo Kim for help with conformation-specific antibodies, and Nir Hacohen and Eric Long for generously providing reagents. We thank the Children's Hospital of Philadelphia Flow Cytometry Core and the University of Pennsylvania Human Immunology Core for time and assistance.

This work was supported by National Institutes of Health grants R01AI065644 and GM104867 (to J.K. Burkhardt) and 5T32AR7442 (to A. Babich).

The authors declare no competing financial interests.

Submitted: 26 June 2014

Accepted: 12 January 2015

## References

- Babich, A., S. Li, R.S. O'Connor, M.C. Milone, B.D. Freedman, and J.K. Burkhardt. 2012. F-actin polymerization and retrograde flow drive sustained PLC $\gamma$ 1 signaling during T cell activation. *J. Cell Biol.* 197:775–787. <http://dx.doi.org/10.1083/jcb.201201018>
- Baker, R.G., C.J. Hsu, D. Lee, M.S. Jordan, J.S. Maltzman, D.A. Hammer, T. Baumgart, and G.A. Koretzky. 2009. The adapter protein SLP-76 mediates “outside-in” integrin signaling and function in T cells. *Mol. Cell Biol.* 29:5578–5589. <http://dx.doi.org/10.1128/MCB.00283-09>
- Beemiller, P., and M.F. Krummel. 2010. Mediation of T-cell activation by actin meshworks. *Cold Spring Harb. Perspect. Biol.* 2:a002444. <http://dx.doi.org/10.1101/cshperspect.a002444>
- Billadeau, D.D., J.C. Nolz, and T.S. Gomez. 2007. Regulation of T-cell activation by the cytoskeleton. *Nat. Rev. Immunol.* 7:131–143. <http://dx.doi.org/10.1038/nri2021>
- Bunnell, S.C., V. Kapoor, R.P. Tribble, W. Zhang, and L.E. Samelson. 2001. Dynamic actin polymerization drives T cell receptor-induced spreading: a role for the signal transduction adaptor LAT. *Immunity.* 14:315–329. [http://dx.doi.org/10.1016/S1074-7613\(01\)00112-1](http://dx.doi.org/10.1016/S1074-7613(01)00112-1)
- Burkhardt, J.K., E. Carrizosa, and M.H. Shaffer. 2008. The actin cytoskeleton in T cell activation. *Annu. Rev. Immunol.* 26:233–259. <http://dx.doi.org/10.1146/annurev.immunol.26.021607.090347>
- Cairo, C.W., R. Mirchev, and D.E. Golan. 2006. Cytoskeletal regulation couples LFA-1 conformational changes to receptor lateral mobility and clustering. *Immunity.* 25:297–308. <http://dx.doi.org/10.1016/j.immuni.2006.06.012>
- Campi, G., R. Varma, and M.L. Dustin. 2005. Actin and agonist MHC-peptide complex-dependent T cell receptor microclusters as scaffolds for signaling. *J. Exp. Med.* 202:1031–1036. <http://dx.doi.org/10.1084/jem.20051182>
- Carman, C.V., and T.A. Springer. 2003. Integrin avidity regulation: are changes in affinity and conformation underemphasized? *Curr. Opin. Cell Biol.* 15:547–556. <http://dx.doi.org/10.1016/j.ceb.2003.08.003>
- Chen, J., W. Yang, M. Kim, C.V. Carman, and T.A. Springer. 2006. Regulation of outside-in signaling and affinity by the  $\beta_2$  I domain of integrin  $\alpha_4\beta_2$ . *Proc. Natl. Acad. Sci. USA.* 103:13062–13067. <http://dx.doi.org/10.1073/pnas.0605666103>



- Chen, W., J. Lou, E.A. Evans, and C. Zhu. 2012. Observing force-regulated conformational changes and ligand dissociation from a single integrin on cells. *J. Cell Biol.* 199:497–512. <http://dx.doi.org/10.1083/jcb.201201091>
- Chen, X., C. Xie, N. Nishida, Z. Li, T. Walz, and T.A. Springer. 2010. Requirement of open headpiece conformation for activation of leukocyte integrin  $\alpha_x\beta_2$ . *Proc. Natl. Acad. Sci. USA.* 107:14727–14732. <http://dx.doi.org/10.1073/pnas.1008663107>
- Choudhuri, K., J. Llodrá, E.W. Roth, J. Tsai, S. Gordo, K.W. Wucherpfennig, L.C. Kam, D.L. Stokes, and M.L. Dustin. 2014. Polarized release of T-cell-receptor-enriched microvesicles at the immunological synapse. *Nature.* 507:118–123. <http://dx.doi.org/10.1038/nature12951>
- Ciobanaru, C., B. Faivre, and C. Le Clainche. 2013. Integrating actin dynamics, mechanotransduction and integrin activation: the multiple functions of actin binding proteins in focal adhesions. *Eur. J. Cell Biol.* 92:339–348. <http://dx.doi.org/10.1016/j.ejcb.2013.10.009>
- Comrie, W., S. Li, S. Boyle, and J.K. Burkhardt. 2015. The dendritic cell cytoskeleton promotes T cell adhesion and activation by constraining ICAM-1 mobility. *J. Cell Biol.* 208:457–473.
- Davis, S.J., and P.A. van der Merwe. 2006. The kinetic-segregation model: TCR triggering and beyond. *Nat. Immunol.* 7:803–809. <http://dx.doi.org/10.1038/ni1369>
- Dransfield, I., and N. Hogg. 1989. Regulated expression of  $Mg^{2+}$  binding epitope on leukocyte integrin  $\alpha$  subunits. *EMBO J.* 8:3759–3765.
- Dustin, M.L. 1998. Making a little affinity go a long way: a topological view of LFA-1 regulation. *Cell Adhes. Commun.* 6:255–262. <http://dx.doi.org/10.3109/15419069809004481>
- Dustin, M.L., T. Starr, R. Varma, and V.K. Thomas. 2007. Supported planar bilayers for study of the immunological synapse. *Curr. Protoc. Immunol.* Chapter 18:Unit 18.13.
- Feigelson, S.W., R. Pasvolsky, S. Cemerski, Z. Shulman, V. Grabovsky, T. Ilani, A. Sagiv, F. Lemaitre, C. Laudanna, A.S. Shaw, and R. Alon. 2010. Occupancy of lymphocyte LFA-1 by surface-immobilized ICAM-1 is critical for TCR- but not for chemokine-triggered LFA-1 conversion to an open headpiece high-affinity state. *J. Immunol.* 185:7394–7404. <http://dx.doi.org/10.4049/jimmunol.1002246>
- Gorman, J.A., A. Babich, C.J. Dick, R.A. Schoon, A. Koenig, T.S. Gomez, J.K. Burkhardt, and D.D. Billadeau. 2012. The cytoskeletal adaptor protein IQGAP1 regulates TCR-mediated signaling and filamentous actin dynamics. *J. Immunol.* 188:6135–6144. <http://dx.doi.org/10.4049/jimmunol.1103487>
- Grakoui, A., S.K. Bromley, C. Sumen, M.M. Davis, A.S. Shaw, P.M. Allen, and M.L. Dustin. 1999. The immunological synapse: a molecular machine controlling T cell activation. *Science.* 285:221–227. <http://dx.doi.org/10.1126/science.285.5425.221>
- Griffiths, G.M., A. Tsun, and J.C. Stinchcombe. 2010. The immunological synapse: a focal point for endocytosis and exocytosis. *J. Cell Biol.* 189:399–406. <http://dx.doi.org/10.1083/jcb.201002027>
- Gross, C.C., J.A. Brzustowski, D. Liu, and E.O. Long. 2010. Tethering of intercellular adhesion molecule on target cells is required for LFA-1-dependent NK cell adhesion and granule polarization. *J. Immunol.* 185:2918–2926. <http://dx.doi.org/10.4049/jimmunol.1000761>
- Hartman, N.C., J.A. Nye, and J.T. Groves. 2009. Cluster size regulates protein sorting in the immunological synapse. *Proc. Natl. Acad. Sci. USA.* 106:12729–12734. <http://dx.doi.org/10.1073/pnas.0902621106>
- Hirata, H., H. Tatsumi, C.T. Lim, and M. Sokabe. 2014. Force-dependent vinculin binding to talin in live cells: a crucial step in anchoring the actin cytoskeleton to focal adhesions. *Am. J. Physiol. Cell Physiol.* 306:C607–C620. <http://dx.doi.org/10.1152/ajpcell.00122.2013>
- Hogg, N., I. Patzak, and F. Willenbrock. 2011. The insider's guide to leukocyte integrin signalling and function. *Nat. Rev. Immunol.* 11:416–426. <http://dx.doi.org/10.1038/nri2986>
- Huang, C., and T.A. Springer. 1997. Folding of the  $\beta$ -propeller domain of the integrin  $\alpha_L$  subunit is independent of the I domain and dependent on the  $\beta_2$  subunit. *Proc. Natl. Acad. Sci. USA.* 94:3162–3167. <http://dx.doi.org/10.1073/pnas.94.7.3162>
- Judokusumo, E., E. Tabdanov, S. Kumari, M.L. Dustin, and L.C. Kam. 2012. Mechanosensing in T lymphocyte activation. *Biophys. J.* 102:L5–L7. <http://dx.doi.org/10.1016/j.bpj.2011.12.011>
- Kaizuka, Y., A.D. Douglass, R. Varma, M.L. Dustin, and R.D. Vale. 2007. Mechanisms for segregating T cell receptor and adhesion molecules during immunological synapse formation in Jurkat T cells. *Proc. Natl. Acad. Sci. USA.* 104:20296–20301. <http://dx.doi.org/10.1073/pnas.0710258105>
- Kim, M., C.V. Carman, and T.A. Springer. 2003. Bidirectional transmembrane signaling by cytoplasmic domain separation in integrins. *Science.* 301:1720–1725. <http://dx.doi.org/10.1126/science.1084174>
- Kim, M., C.V. Carman, W. Yang, A. Salas, and T.A. Springer. 2004. The primacy of affinity over clustering in regulation of adhesiveness of the integrin  $\alpha_L\beta_2$ . *J. Cell Biol.* 167:1241–1253. <http://dx.doi.org/10.1083/jcb.200404160>
- Kinashi, T. 2005. Intracellular signalling controlling integrin activation in lymphocytes. *Nat. Rev. Immunol.* 5:546–559. <http://dx.doi.org/10.1038/nri1646>
- Kong, F., A.J. García, A.P. Mould, M.J. Humphries, and C. Zhu. 2009. Demonstration of catch bonds between an integrin and its ligand. *J. Cell Biol.* 185:1275–1284. <http://dx.doi.org/10.1083/jcb.200810002>
- Kong, F., Z. Li, W.M. Parks, D.W. Dumbauld, A.J. García, A.P. Mould, M.J. Humphries, and C. Zhu. 2013. Cyclic mechanical reinforcement of integrin–ligand interactions. *Mol. Cell.* 49:1060–1068. <http://dx.doi.org/10.1016/j.molcel.2013.01.015>
- Kumari, S., S. Vardhana, M. Cammer, S. Curado, L. Santos, M.P. Sheetz, and M.L. Dustin. 2012. T lymphocyte myosin IIA is required for maturation of the immunological synapse. *Front. Immunol.* 3:230. <http://dx.doi.org/10.3389/fimmu.2012.00230>
- Lefort, C.T., Y.M. Hyun, J.B. Schultz, F.Y. Law, R.E. Waugh, P.A. Knauf, and M. Kim. 2009. Outside-in signal transmission by conformational changes in integrin Mac-1. *J. Immunol.* 183:6460–6468. <http://dx.doi.org/10.4049/jimmunol.0900983>
- Li, D., J.J. Moldrem, and Q. Ma. 2009. LFA-1 regulates CD8<sup>+</sup> T cell activation via T cell receptor-mediated and LFA-1-mediated Erk1/2 signal pathways. *J. Biol. Chem.* 284:21001–21010. <http://dx.doi.org/10.1074/jbc.M109.002865>
- Li, Y.C., B.M. Chen, P.C. Wu, T.L. Cheng, L.S. Kao, M.H. Tao, A. Lieber, and S.R. Roffler. 2010. Cutting edge: mechanical forces acting on T cells immobilized via the TCR complex can trigger TCR signaling. *J. Immunol.* 184:5959–5963. <http://dx.doi.org/10.4049/jimmunol.0900775>
- Liu, B., W. Chen, B.D. Evavold, and C. Zhu. 2014. Accumulation of dynamic catch bonds between TCR and agonist peptide-MHC triggers T cell signaling. *Cell.* 157:357–368. <http://dx.doi.org/10.1016/j.cell.2014.02.053>
- Lu, C., M. Ferzly, J. Takagi, and T.A. Springer. 2001. Epitope mapping of antibodies to the C-terminal region of the integrin  $\beta_2$  subunit reveals regions that become exposed upon receptor activation. *J. Immunol.* 166:5629–5637. <http://dx.doi.org/10.4049/jimmunol.166.9.5629>
- Ma, Z., K.A. Sharp, P.A. Janmey, and T.H. Finkel. 2008. Surface-anchored monomeric agonist pMHCs alone trigger TCR with high sensitivity. *PLoS Biol.* 6:e43.
- March, M.E., and E.O. Long. 2011.  $\beta_2$  integrin induces TCR $\zeta$ -Syk-phospholipase C- $\gamma$  phosphorylation and paxillin-dependent granule polarization in human NK cells. *J. Immunol.* 186:2998–3005. <http://dx.doi.org/10.4049/jimmunol.1002438>
- Margadant, F., L.L. Chew, X. Hu, H. Yu, N. Bate, X. Zhang, and M. Sheetz. 2011. Mechanotransduction in vivo by repeated talin stretch-relaxation events depends upon vinculin. *PLoS Biol.* 9:e1001223. <http://dx.doi.org/10.1371/journal.pbio.1001223>
- Monks, C.R., B.A. Freiberg, H. Kupfer, N. Sciaky, and A. Kupfer. 1998. Three-dimensional segregation of supramolecular activation clusters in T cells. *Nature.* 395:82–86. <http://dx.doi.org/10.1038/25764>
- Morin, N.A., P.W. Oakes, Y.M. Hyun, D. Lee, Y.E. Chin, M.R. King, T.A. Springer, M. Shimaoka, J.X. Tang, J.S. Reichner, and M. Kim. 2008. Nonmuscle myosin heavy chain IIA mediates integrin LFA-1 de-adhesion during T lymphocyte migration. *J. Exp. Med.* 205:195–205. (published erratum appears in *J. Exp. Med.* 2008. 205:993.) <http://dx.doi.org/10.1084/jem.20071543>
- Nguyen, K., N.R. Sylvain, and S.C. Bunnell. 2008. T cell costimulation via the integrin VLA-4 inhibits the actin-dependent centralization of signaling microclusters containing the adaptor SLP-76. *Immunity.* 28:810–821. <http://dx.doi.org/10.1016/j.immuni.2008.04.019>
- Nishida, N., C. Xie, M. Shimaoka, Y. Cheng, T. Walz, and T.A. Springer. 2006. Activation of leukocyte  $\beta_2$  integrins by conversion from bent to extended conformations. *Immunity.* 25:583–594. <http://dx.doi.org/10.1016/j.immuni.2006.07.016>
- Nolz, J.C., R.B. Medeiros, J.S. Mitchell, P. Zhu, B.D. Freedman, Y. Shimizu, and D.D. Billadeau. 2007. WAVE2 regulates high-affinity integrin binding by recruiting vinculin and talin to the immunological synapse. *Mol. Cell Biol.* 27:5986–6000. <http://dx.doi.org/10.1128/MCB.00136-07>
- O'Connor, R.S., X. Hao, K. Shen, K. Bashour, T. Akimova, W.W. Hancock, L.C. Kam, and M.C. Milone. 2012. Substrate rigidity regulates human T cell activation and proliferation. *J. Immunol.* 189:1330–1339. <http://dx.doi.org/10.4049/jimmunol.1102757>
- Partridge, A.W., S. Liu, S. Kim, J.U. Bowie, and M.H. Ginsberg. 2005. Transmembrane domain helix packing stabilizes integrin  $\alpha_{IIb}\beta_3$  in the low affinity state. *J. Biol. Chem.* 280:7294–7300. <http://dx.doi.org/10.1074/jbc.M412701200>
- Perez, O.D., D. Mitchell, G.C. Jager, S. South, C. Murriel, J. McBride, L.A. Herzenberg, S. Kinoshita, and G.P. Nolan. 2003. Leukocyte functional antigen 1 lowers T cell activation thresholds and signaling through cytohesin-1 and Jun-activating binding protein 1. *Nat. Immunol.* 4:1083–1092. <http://dx.doi.org/10.1038/ni984>



- Riedl, J., A.H. Crevenna, K. Kessenbrock, J.H. Yu, D. Neukirchen, M. Bista, F. Bradke, D. Jenne, T.A. Holak, Z. Werb, et al. 2008. Lifeact: a versatile marker to visualize F-actin. *Nat. Methods*. 5:605–607. <http://dx.doi.org/10.1038/nmeth.1220>
- Schürpf, T., and T.A. Springer. 2011. Regulation of integrin affinity on cell surfaces. *EMBO J.* 30:4712–4727. <http://dx.doi.org/10.1038/emboj.2011.333>
- Shimaoka, M., T. Xiao, J.H. Liu, Y. Yang, Y. Dong, C.D. Jun, A. McCormack, R. Zhang, A. Joachimiak, J. Takagi, et al. 2003. Structures of the  $\alpha$ L I domain and its complex with ICAM-1 reveal a shape-shifting pathway for integrin regulation. *Cell*. 112:99–111. [http://dx.doi.org/10.1016/S0092-8674\(02\)01257-6](http://dx.doi.org/10.1016/S0092-8674(02)01257-6)
- Sims, T.N., T.J. Soos, H.S. Xenias, B. Dubin-Thaler, J.M. Hofman, J.C. Waite, T.O. Cameron, V.K. Thomas, R. Varma, C.H. Wiggins, et al. 2007. Opposing effects of PKC $\theta$  and WASp on symmetry breaking and relocation of the immunological synapse. *Cell*. 129:773–785. <http://dx.doi.org/10.1016/j.cell.2007.03.037>
- Smith, A., Y.R. Carrasco, P. Stanley, N. Kieffer, F.D. Batista, and N. Hogg. 2005. A talin-dependent LFA-1 focal zone is formed by rapidly migrating T lymphocytes. *J. Cell Biol.* 170:141–151. <http://dx.doi.org/10.1083/jcb.200412032>
- Springer, T.A., and M.L. Dustin. 2012. Integrin inside-out signaling and the immunological synapse. *Curr. Opin. Cell Biol.* 24:107–115. <http://dx.doi.org/10.1016/j.ccb.2011.10.004>
- Suzuki, J., S. Yamasaki, J. Wu, G.A. Koretzky, and T. Saito. 2007. The actin cloud induced by LFA-1-mediated outside-in signals lowers the threshold for T-cell activation. *Blood*. 109:168–175. <http://dx.doi.org/10.1182/blood-2005-12-020164>
- Tabassam, F.H., H. Umehara, J.Y. Huang, S. Gouda, T. Kono, T. Okazaki, J.M. van Seventer, and N. Domae. 1999.  $\beta_2$ -integrin, LFA-1, and TCR/CD3 synergistically induce tyrosine phosphorylation of focal adhesion kinase (pp125<sup>FAK</sup>) in PHA-activated T cells. *Cell. Immunol.* 193:179–184. <http://dx.doi.org/10.1006/cimm.1999.1472>
- Tadokoro, S., S.J. Shattil, K. Eto, V. Tai, R.C. Liddington, J.M. de Pereda, M.H. Ginsberg, and D.A. Calderwood. 2003. Talin binding to integrin  $\beta$  tails: a final common step in integrin activation. *Science*. 302:103–106. <http://dx.doi.org/10.1126/science.1086652>
- Takagi, J., B.M. Petre, T. Walz, and T.A. Springer. 2002. Global conformational rearrangements in integrin extracellular domains in outside-in and inside-out signaling. *Cell*. 110:599–611. [http://dx.doi.org/10.1016/S0092-8674\(02\)00935-2](http://dx.doi.org/10.1016/S0092-8674(02)00935-2)
- Thauland, T.J., and D.C. Parker. 2010. Diversity in immunological synapse structure. *Immunology*. 131:466–472. <http://dx.doi.org/10.1111/j.1365-2567.2010.03366.x>
- Thomas, W.E., V. Vogel, and E. Sokurenko. 2008. Biophysics of catch bonds. *Annu. Rev. Biophys.* 37:399–416. <http://dx.doi.org/10.1146/annurev.biophys.37.032807.125804>
- Vardhana, S., K. Choudhuri, R. Varma, and M.L. Dustin. 2010. Essential role of ubiquitin and TSG101 protein in formation and function of the central supramolecular activation cluster. *Immunity*. 32:531–540. <http://dx.doi.org/10.1016/j.immuni.2010.04.005>
- Varga, G., N. Nippe, S. Balkow, T. Peters, M.K. Wild, S. Seeliger, S. Beissert, M. Krummen, J. Roth, C. Sunderkötter, and S. Grabbe. 2010. LFA-1 contributes to signal I of T-cell activation and to the production of T<sub>H</sub>1 cytokines. *J. Invest. Dermatol.* 130:1005–1012. <http://dx.doi.org/10.1038/jid.2009.398>
- Varma, R., G. Campi, T. Yokosuka, T. Saito, and M.L. Dustin. 2006. T cell receptor-proximal signals are sustained in peripheral microclusters and terminated in the central supramolecular activation cluster. *Immunity*. 25:117–127. <http://dx.doi.org/10.1016/j.immuni.2006.04.010>
- Wang, H., B. Wei, G. Bismuth, and C.E. Rudd. 2009. SLP-76-ADAP adaptor module regulates LFA-1 mediated costimulation and T cell motility. *Proc. Natl. Acad. Sci. USA*. 106:12436–12441. <http://dx.doi.org/10.1073/pnas.0900510106>
- Xie, J., J.B. Huppa, E.W. Newell, J. Huang, P.J. Ebert, Q.J. Li, and M.M. Davis. 2012. Photocrosslinkable pMHC monomers stain T cells specifically and cause ligand-bound TCRs to be ‘preferentially’ transported to the cSMAC. *Nat. Immunol.* 13:674–680. <http://dx.doi.org/10.1038/ni.2344>
- Yi, J., X.S. Wu, T. Crites, and J.A. Hammer III. 2012. Actin retrograde flow and actomyosin II arc contraction drive receptor cluster dynamics at the immunological synapse in Jurkat T cells. *Mol. Biol. Cell*. 23:834–852. <http://dx.doi.org/10.1091/mbc.E11-08-0731>
- Yokosuka, T., K. Sakata-Sogawa, W. Kobayashi, M. Hiroshima, A. Hashimoto-Tane, M. Tokunaga, M.L. Dustin, and T. Saito. 2005. Newly generated T cell receptor microclusters initiate and sustain T cell activation by recruitment of Zap70 and SLP-76. *Nat. Immunol.* 6:1253–1262. <http://dx.doi.org/10.1038/ni1272>
- Yu, Y., A.A. Smoligovets, and J.T. Groves. 2013. Modulation of T cell signaling by the actin cytoskeleton. *J. Cell Sci.* 126:1049–1058. <http://dx.doi.org/10.1242/jcs.098210>
- Zhu, J., C.V. Carman, M. Kim, M. Shimaoka, T.A. Springer, and B.H. Luo. 2007. Requirement of  $\alpha$  and  $\beta$  subunit transmembrane helix separation for integrin outside-in signaling. *Blood*. 110:2475–2483. <http://dx.doi.org/10.1182/blood-2007-03-080077>
- Zhu, J., B.H. Luo, T. Xiao, C. Zhang, N. Nishida, and T.A. Springer. 2008. Structure of a complete integrin ectodomain in a physiologic resting state and activation and deactivation by applied forces. *Mol. Cell*. 32:849–861. <http://dx.doi.org/10.1016/j.molcel.2008.11.018>
- Zhu, J., J. Zhu, and T.A. Springer. 2013. Complete integrin headpiece opening in eight steps. *J. Cell Biol.* 201:1053–1068. <http://dx.doi.org/10.1083/jcb.201212037>